The Thesis Committee for Prateek Bhardwaj
Certifies that this is the approved version of the following thesis:

A New Reservoir Scale Model for Fracture Propagation and Stress Reorientation in Waterflooded Reservoirs

APPROVED BY
SUPERVISING COMMITTEE:

Supervisor:

Mukul M. Sharma

Jon E. Olson

A New Reservoir Scale Model for Fracture Propagation and Stress Reorientation in Waterflooded Reservoirs

by

Prateek Bhardwaj, B.E.

Thesis

Presented to the Faculty of the Graduate School of

The University of Texas at Austin

in Partial Fulfillment

of the Requirements

for the Degree of

Master of Science in Engineering

The University of Texas at Austin

December 2016

Dedication

To my parents, who always stress on being a good person more than anything else.

To my sister, for her unconditional love and support.

Acknowledgements

I am sincerely thankful to Dr. Mukul M Sharma for giving me the opportunity to work as a member of his research group. The constant guidance and support provided by him has been an integral to the successful completion of this work. I would like to acknowledge the funding and support from the member companies of the Hydraulic Fracturing and Sand Control Joint Industry Consortium at the University of Texas at Austin, due to which this research was made possible.

I feel lucky to have been part of the wonderful hydraulic fracturing modeling research group. I am extremely thankful to Eric, Ripudaman, Hisanao, Jongsoo, Dongkeun, and Haotian for all their unconditional support in getting through the steep learning curve, and introducing me to the world of numerical modeling and geomechanics. I am deeply indebted to Dr. Philip Cardiff for his patience in helping me understand even the most basic things. I am thankful to Jin for having solutions to all possible problems a student can have. I couldn't have asked for better colleagues or work environment.

I am grateful my friends, Vasundhara and Rahul, for their constant encouragement throughout this journey. I extend my sincere gratitude to my family and friends back home who have been extremely patient with me during this period of my life. I feel lucky to have had the endless love and support of my parents, Manju and Mukesh Bhardwaj and loveliest sister Nishu, who never made me feel away from home.

Abstract

A New Reservoir Scale Model for Fracture Propagation and Stress Reorientation in Waterflooded Reservoirs

Prateek Bhardwaj, M.S.E.

The University of Texas at Austin, 2016

Supervisor: Mukul M. Sharma

It is now well established that poro-thermo-elastic effects substantially change the magnitude and orientation of in-situ stresses. Fractures induced in injectors during water injection for waterflooding or produced water disposal have a profound impact on waterflood performance. These effects, coupled with injectivity decline due to plugging caused by injected particles, lead to permeability reduction, fracture initiation and propagation. Models are available for fracture propagation in single injection wells and single layered reservoirs that account for these effects. However, the impact of fluid injection and production on fracture growth in multiple wells and multi-layered reservoirs with competing fractures, has not been systematically modelled at a field scale.

In this work, a three-dimensional, two-phase flow simulator with iteratively coupled geomechanics has been developed and applied to model the dynamic growth of injection-induced fractures. The model is based on a finite volume implementation of the cohesive zone model for arbitrary fracture propagation coupled with two-phase flow. A dynamic filtration model for permeability reduction is employed on the fracture faces to

incorporate effects of internal damage and external filter cake build-up due to the injection of suspended solids and oil droplets. All physical phenomena are solved in a single framework designed for multi-well, field-scale simulation.

The pressure distribution, saturation profile, thermal front, mechanical displacements and reservoir stresses are computed as fluids are injected and produced from the reservoir. Simulation results are discussed with single as well as multiple fractures propagating. Stress reorientation due to poroelastic, thermoelastic and mechanical effects is examined for the simulated cases. The orientation of the fractures is controlled primarily by the orientation of the stresses, which in turn depends on the pattern of wells and the rates of injection and production. The sweep efficiency of the waterflood is found to be impacted by the rate of growth of injection-induced fractures. Heterogeneities in multi-layered reservoirs strongly govern the expected vertical sweep and fluid distribution, which impacts the cumulative oil recovery.

This is the first time a formulation of multiphase flow in the reservoir has been coupled with dynamic fracture propagation in multiple wells induced by solids plugging while including poro-thermo-elasticity at the reservoir scale. The model developed in this work can be used to simulate multiple water injection induced fractures, determine the reoriented stress state to optimize the location of infill wells and adjust injection well patterns to maximize reservoir sweep.

Table of Contents

List of Tables

List of Figures

Chapter 1: Introduction

1.1. Problem Description

Water injection is one the most common activities in an oilfield. It may be employed in the form of a secondary recovery mechanism, as a base fluid for enhanced oil recovery methods, for voidage replacement, disposal or reinjection of produced water. The injected water is typically treated prior to injection, but despite surface filtration and treatment, abundant quantities of water injected every day for several years accumulates large volumes of fines, oil droplets and solid particles being injected. To get an estimate number for the quantity of injected particles in a typical injection well over its life, consider a well injecting at 10,000bbl/d, with injection fluid at a particle concentration of 10 ppm. The mass of particles injected per year approximately amounts to:

$$\text{Rate of particle injection } = \left(\frac{10{,}000\ bbl}{day}\right)\left(\frac{10\ mg}{l}\right)\left(\frac{158.9\ l}{bbl}\right)$$
$$= 1.589\times10^{7}\ \frac{mg}{day} \approx 16\ \frac{kg}{day} \approx 5.8\ \frac{ton}{yr} \qquad (1.1)$$

The operating bottomhole pressure in water injectors is governed by many factors. A suitable injection schedule is planned based on the volumes of fluid that can be injected. This significant amount of injected suspended solids can potentially plug the near wellbore region and formation, leading to a gradual buildup of the bottomhole flowing pressures. Over several years of injection, this plugging leads to a decline in injectivity (I), given by Eq. 1.2, resulting from the higher bottomhole flowing pressures (P_{wf}).

$$I = \frac{Q_T}{P_{wf} - P_R} \qquad (1.2)$$

Here, Q_T is the total injection rate P_R is the average reservoir pressure at the boundary.

The time scale of water injection, which spans several years, makes poroelastic, thermoelastic and mechanical effects significant at the reservoir scale.

- ***Poroelastic Effects***: Fluid injection and production gives rise to increasing or decreasing pore pressure and pore pressure gradients in the field which results in poroelastic effects in the reservoir. For example, fluid injection increases the pore pressure in the formation and creates high pore pressure gradients around the injection well. Since the fluid in the pores supports the rock matrix in counter balancing the total stress, the injection of fluids into pores reduces the effective compressive stress in the matrix. A similar and opposite effect is observed due to fluid production. Therefore, poroelastic effects of fluid injection and production affect the magnitude and orientation of in-situ stresses.
- ***Thermoelastic Effects:*** Another significant aspect of water injection is thermal effects of cold fluid injection. It is common in the field, to inject relatively cold water into typically hot reservoirs. When cold fluid comes in contact with the formation rock, the rock to contract, which results in a reduction of compressive stresses in the matrix. Thus, thermal stresses can also become significant.
- ***Mechanical Effects:*** If injection is below the fracture pressure gradient, near wellbore formation damage, internal and external filtration leads to a buildup in the bottomhole pressure which may exceed the fracture gradient. Hence, almost all water injectors are fractured at some stage in their life. Mechanical effects can affect the stress state and are a result of rock failure or deformation. For example, fracture opening will lead to a locally elevated stress perpendicular to the fracture face. The stress state around one fracture can affect other fractures in potential

infill well locations. Thus, mechanical deformation of the matrix becomes another significant aspect of the water injection process.

Field studies and experimental work have established that poroelastic and thermoelastic effects, coupled with injectivity decline due to plugging and filtration caused by suspended particles in injection water, lead to permeability reduction, fracture initiation and propagation in water injectors (Sharma et al., 2000).

However, reservoir simulators do not account for propagating fractures during water injection, which can significantly impact the recovery and intended sweep of the waterflood, especially in multilayered reservoirs. Induced fracture propagation is primarily governed by injected solids plugging and permeability decline over extended periods of water injection. Additionally, stress reorientation due to poroelastic and thermoelastic effects of fluid injection and production substantially change the magnitude and orientation of in-situ stresses. Thus in most wells, injection above the fracture pressure gradient leads to fracture propagation. Although fractured injectors demonstrate better injectivity, it is imperative to understand the primary factors that control the process, in order to address critical issues such as fracture containment in the intended zone and impact on reservoir sweep. This makes modeling the process indispensable in early stages of field development. Since this process is a combination of several macro and micro scale phenomena, past work has often been focused on studying these phenomena independently while making simplifying assumptions for the others. A simulator which can account for poroelasticity, thermoelasticity, fracture propagation, particle filtration along with two phase reservoir flow in the reservoir domain is expected to give a more accurate depiction of the physical phenomena.

1.2. Thesis outline

This work describes the development of a coupled geomechanical reservoir simulator, with filtration and thermal effects included in a three dimensional poro-thermo-elastic reservoir domain. An Implicit Pressure Explicit Saturation (IMPES) formulation was used to implement two phase flow in the reservoir domain, with pressure coupled with mechanical displacement using Biot's theory of poroelasticity. Thermal effects of fluid injection were incorporated using an energy balance approach. One way coupling is implemented for temperature with pressure and temperature with mechanical displacement, to account for thermoelastic effects. The fluid flow model was then coupled with the finite volume cohesive zone model for arbitrary fracture propagation. A filtration model to account for the fracture plugging and subsequent propagation was added to the formulation. Well models were implemented to simulate multi-well cases, and multiple fracture propagation with and without flow distribution was modelled.

Chapter 2 presents a thorough literature review of past developments in modelling water injection induced fractures. The present status of development and limitations of the past research are discussed. Unresolved issues are identified to explore knowledge gaps which led to the formulation implemented in this work. Chapter 3 describes the implementation of poroelasticity, thermoelasticity, two phase flow, fracture propagation and particle filtration models. The coupling of these phenomenon and the governing equations for pressure, saturation, displacement and temperature are discussed. The introduction of the coupling of the primary field variables is followed by a brief description of the finite volume cohesive zone model for arbitrary fracture propagation. The development of the particle filtration model in the current implementation of this work is discussed. The algorithm of the implementation is then discussed. The two phase

flow model is verified with Buckley-Leverett analytical solution for one dimensional flow. The results obtained using the simulator developed are discussed in Chapter 4. The discussion comprises of a study of critical factors affecting the phenomenon of injection induced fractures and potential field applications of the model developed in this work. The conclusion of the work is presented in Chapter 5.

Figures

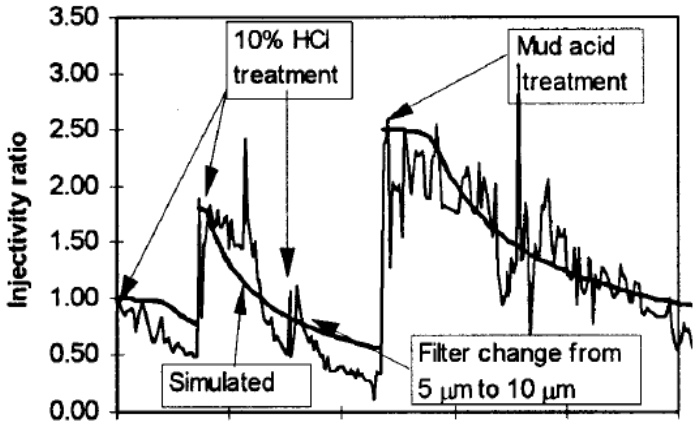

Figure 1.1: Injectivity decline in a typical water injection well in offshore Gulf of Mexico (Sharma et al., 2000).

Chapter 2: Literature Review

Injection induced fracture propagation is a combination of a number of near wellbore scale and field scale phenomena, in addition to the mechanics associated with fracture propagation. Primarily, particle filtration and plugging governs fracture propagation over several years of injection. A large quantity of injected solids drives the propagation of these slower propagating fractures. Since the in-situ stress state is reoriented due to extended periods of fluid injection and production, it is important to compute these changes. The critical aspects of modeling the injection induced fracturing process are:

- Particle Plugging and Filtration
- Fracture Propagation
- Height Containment
- Thermal Effects of Water Injection
- Stress Reorientation.

The work done in the respective areas is reviewed in this chapter. These physical processes have been systematically studied by researchers in the past, often individually, with simplified assumptions for the other factors. However, modeling injection induced fractures requires all these phenomenon to be taken into account. The work done in the respective areas is reviewed in this chapter.

2.1. Particle plugging and filtration in injection induced fractures

Loss in well injectivity and subsequent bottomhole pressure build up is attributed to suspended particles plugging the near wellbore region. Barkman & Davidson (1972) showed that injectivity decline is a direct function of water quality. Eylander (1988) also

presented a method to predict injectivity decline, but these models required the invasion depth and internal filter cake permeability to be specified a priori. van Oort et al. (1993) described inflow velocity and particle/pore size effects of injection to improve impairment models through core flood experiments. However, these models treated internal and external filtration separately.

Particle plugging occurs in two stages, internal and external filtration. After the formation is plugged internally, a filter cake starts building up on the surface of the rock. A transition time was defined by Pang and Sharma (1997) after which the injected particles can no longer plug the formation internally and an external filter cake deposition commences (Figure 2.1). Wennberg & Sharma (1997) used the concept of filtration coefficient, and their implementation improved the predictions of the rate of internal filtration, transition time to external filtration. The permeability reduction model proposed by Sharma et al. (2000) predicts the permeability profiles resulting from particle plugging of the rock and the fracture face.

2.2. Induced fracture propagation models

Fracture propagation in water injectors differs significantly from conventional hydraulic fracture treatments. Though the mechanics of fracture propagation models can be applied, the propagation is governed by a slow and gradual permeability decline at the fracture faces due to particle plugging as opposed to high injection pressure in hydraulic fracture treatments. The time scale of propagation is of the order of years and it is necessary to model the formation damage and filtration process. In the past, researchers have attempted to combine fracture propagation models with the physics of filtration or used analytical fracture models with a focus on formation damage or reservoir flow.

Hagoort et al. (1980) proposed a mathematical model to simulate the propagation of waterflood-induced hydraulic fractures in a symmetry element of a waterflood pattern. It consisted of a conventional single-phase reservoir simulator coupled with an analytical fracture model. Pang and Sharma (1995) developed single well injector models for predicting injectivity decline and near wellbore formation damage for open-hole, perforated and fractured water injectors. Pang and Sharma (1997) and Wennberg and Sharma (1997) developed a comprehensive water injection model based on Perkins and Gonzales (1985) model. Perkins and Gonzales had developed a numerical method to calculate thermoelastic stresses induced within elliptically shaped regions of finite thickness (Figure 2.2). Various improvements were made by Suri et al. (2011) to this model. An improved internal filtration model by Gadde and Sharma (2001) was included to calculate permeability reduction and the dynamic process of fracture growth and filtration was simplified as a pseudo static process. The fluid flow and relevant pressure drops for composite reservoir zones were based on the infinite conductivity solution by Gringarten et al. (1974). The dimensions and pressure drops of the stepwise fluid and thermal fronts are analytically calculated, assuming a vertical bi-wing fracture. The fluid and thermal fronts are assumed to be ellipses confocal with the fracture. For the fracture growth calculation used in water injection models, Perkins and Gonzales predicted the changes in in-situ stress by thermoelastic and poroelastic effect induced by long-term injection. These models were combined into a semi-analytical numerical simulation to simulate fractured or unfractured vertical open-hole gravel-packed wells, cased and perforated wells, horizontal wells with transverse or longitudinal fractures by Suri and Sharma (2009), and vertical frac-packed well by Suri and Sharma (2010). Suri et al.

(2011) estimated fracture length in horizontal wells by performing a history match by taking pressure transient effects into account.

2.3. Height containment models

Due to the long term injection and high fluid volumes injected, it becomes necessary to plan the injection schedule by taking into account the cap rock stress. Height containment of fractures is an issue with severe economic and environmental consequences. If the induced fracture in the target sand breaches the bounding shale, the injected fluid can potentially be lost to the bounding layer. In an offshore scenario, if the induced fractures grow to the seabed, the environmental consequences can be extremely severe. The time for the induced fracture to reach the bounding layer when it is initiated is not negligible in thick zones (Abou-Sayed et al., 1984) but conventional fracture models such as PKN assume a constant height. Fracture containment cannot be modeled by using these 2-D models which constrain the height of the fracture to the pay zone.

Simonson et al. (1978) studied containment of hydraulic fractures and growth direction in height through three cases; different material properties, effect of in-situ stress variations and pressure gradients effect of fracturing fluids. They based their study on the investigation of linear elastic fracture mechanics formulations restricted by analytical solutions and simplified assumptions. van Eekelen (1982) investigated the shape of fracture penetration for height growth into the bounding layers. Height growth and penetration were observed to be dependent on stiffness and in-situ stress contrast. Fung et al. (1987) applied an analytic procedure for calculating vertical fracture extent in symmetrical tri-layered formations, which was extended to multilayered, asymmetrical formations using a semi-analytic technique. Gu (1987) and Yew (1997) considered the

problem of the opening displacement of a mode-I planar fracture in an infinite elastic medium. Based on a finite element formulation for the fluid flow equation in a fracture and the fracture opening equation, they developed the iterative scheme for the 3-D fracture propagation calculation for hydraulic fracturing simulations. Hwang (2014) developed a 3-D implementation of this model to address fracture containment of water injection induced fractures. The strong dependence of fracture containment on stress contrast was simulated (Figure 2.3). The model was modified to accommodate the time scale of water injection, which normally extends to several years. The fracture model solves the fracture opening equation and the fluid flow equation in the fracture. However, it is limited to a single well and a single fracture propagation in a pre-defined plane.

2.4. Stress reorientation during waterflooding

Stress reorientation during waterflooding can be a critical factor since it controls the orientation of the induced fracture. Dikken & Niko (1987) investigated the effect of waterflood-induced fracture propagation on reservoir sweep. Fracture growth was calculated using the concept of a critical stress intensity factor. Both poroelastic and thermoelastic changes in the horizontal stresses are calculated numerically and their influence on the fracture initiation/propagation is continuously taken into account. A model of fracture wall impairment because of filter-cake build-up due to poor quality injection water is included. Gadde & Sharma (2001) investigated the role of injection induced fractures on waterflooding oil recovery efficiency. They showed that the growth of such fractures could be adequately modeled using an explicit formulation that coupled fracture growth to the change in pressure due to injected solids. Fracture growth was

shown to have a significant impact on oil recovery in multi-layered reservoirs. However, the stress field in the reservoir was not computed.

Wright et al. (1995), explained stress reorientation by three mechanisms: reservoir compaction, poroelastic effects, and fault-slip effects. They proposed a strategy for detecting and possibly mitigating some of the adverse effects of production/injection induced reservoir stress changes - reservoir compaction and surface subsidence as well as fracture reorientation. Dons et al. (2007) showed that the seismic responses induced by fluid substitution and pressure gradients during long-term waterflooding can be interpreted as rock hardening and softening. This illustrated the field-wide response of stress changes due to fluid injection. Hwang et al. (2015) developed a model that showed that stress-reorientation during waterflooding is not a near-well phenomenon, but instead occurs on a field scale. Even for simple five-spot models, the complete reversal of the maximum and minimum horizontal stress directions can occur far from injection/production wells. The contrast between horizontal stresses also changes significantly, indicating locations where natural fracture networks are likely to be stimulated. They also showed that for horizontal wells, the stress reorientation can be fairly non-intuitive, with the maximum horizontal stress aligning parallel to the injector as opposed to the expected perpendicular outwards direction computed in vertical wells. They combined poroelastic effects with thermoelastic effects in a coupled formulation to determine stress state in injector well pairs (Figure 2.4).

2.5. Thermal effects

Injection of cold fluid into hot reservoirs, which is a common scenario for injectors, introduces thermoelastic effects in the reservoir. Injecting cold fluid in a hot

formation leads to contraction of the rock matrix, thereby leading to the development of tensile thermal stresses. The thermally induced tensile stress oppose the compressive effects of fluid injection and help in propagation of the fracture, by reducing the horizontal stresses in the reservoir. Hot water injection will have the opposite effect of rock expansion and would increase the compressive stress in the matrix. If the temperature of the injected water is different from the reservoir temperature, it can have a significant effect on fluid properties such as viscosity, which directly impacts the mobility ratio between the displacing and displaced fluid. Thermoelastic effects become extremely significant in water flooding induced fractures due to the time scale of injection, which facilitates propagation of a thermal front behind the saturation front.

Perkins & Gonzalez (1985) built a fractured-well model with elliptical thermal and waterflood fronts. The reservoir flow and temperature was semi-analytically described, and the thermal stress change was calculated. This calculation has been used in numerous models to apply fracture growth predictions. Martins et al. (1995) did an analysis of about 159 injectors from the Prudhoe Bay oilfield that were subjected to periods of injection with sea water and produced water. The long-term effects on injection performance of produced-water quality, fluid temperature, fracture growth, well trajectory, and other factors were quantified. Thermally induced fracturing was found to be one of the main reasons for the high injectivity maintained for long periods of time. Comparison of cooler sea water (80^{o}F) injection which was alternated with produced water (150^{o}F) confirmed the effect of thermal stresses. It was also shown that the thermally induced stress change can sometimes promote fracture growth into bounding layers, which can impact the waterflooding efficiency due to conduction to adjacent layers. Detienne et al. (1998) used a filter cake and internal damage model to predict

injection well performance. He applied a semi-analytic method for thermal stress changes. In their work they observed that for hot water injection the fractures would shrink but the higher fluid temperature reduced the fluid viscosity, hence, enhancing the mobility of the injected fluid. They concluded that at medium contaminant concentrations, high water temperatures improve water viscosity and tend to maintain the injectivity despite the damage by suspended solids and fracture shrinkage.

DISCUSSION OF PRESENT STATUS AND UNRESOLVED ISSUES

A simulator that can account for poroelasticity, thermoelastcity, fracture propagation, and particle filtration along with two phase reservoir flow in the reservoir domain, is expected to give a more accurate depiction of the physical processes that control injector performance, oil recovery and fracture growth. These physical processes have been systematically studied by researchers in the past, often individually, but with simplified assumptions for the others. However, modeling the process of induced fracture propagation and oil recovery requires all these phenomena to be taken into account. Each process impacts the other, which necessitates coupling these effects together. Fracture propagation models used to simulate injection induced fractures are based on linear elastic formulation with the effects of poroelastic and thermoelastic stresses often included explicitly using semi-analytical methods. It may be significant to couple mechanical effects of fracture opening with the above in an iteratively coupled formulation for pressure and displacement to capture effects such as stress interference between wells and poroelastic back stresses.

- Models are available for fracture propagation in single injection wells and single layered reservoirs to account for these effects. However, the impact of fluid

injection and production on fracture growth in multiple wells and multi-layered reservoirs with competing fractures, has not been systematically modelled at a field scale.

- Water injection can be done in the oil leg of the reservoir or the aquifer. Water injection induced fracture simulation in the oil leg make it necessary to simulate at least two fluid phases in the reservoir. Current fracture propagation models are either limited to one phase flow in the reservoir, or assume a simple piston like displacement of the displacing fluid. Buckley Leverette type front displacement is not included in any of the current models for water injection induced fractures.
- Current models have a pre-defined propagation path and/or are restricted to a single plane of propagation. Fracture turning is not allowed. This is likely to occur in the case of induced fractures approaching depleted regions around producers or interacting with other induced fractures in the same well. Arbitrary fracture propagation has not been modelled in a three-dimensional poroelastic and thermoelastic reservoir domain.
- Coupled reservoir simulation and geomechanics has been studied and simulators have been developed to accommodate geomechanical effects on porosity and permeability. Although simulators account for two-phase flow, propagating fractures are unaccounted for in terms of the impact on reservoir sweep, oil recovery and water breakthrough.
- In injection wells, fracture propagation is primarily governed by particle plugging and filtration at the fracture faces. Fracture orientation, on the other hand, is governed by in-situ horizontal stress directions. Fracture propagation dynamically coupled with permeability decline due to filtration and reservoir stress

reorientation, needs to be integrated as changes in stress orientation can impact the direction of the induced fractures.

- Fracture containment by bounding layers, when not properly addressed, may significantly distort all aspects of the mechanical and fluid flow behavior. Water injection over a long period of time presents the risk of significant in-situ stress reorientation. Once a fracture starts to grow into bounding layers, the sweep efficiency of water flooding will be seriously compromised. It is necessary to predict the potential breach of the fracture into the bounding shale during the planning of the water flood.

Figures

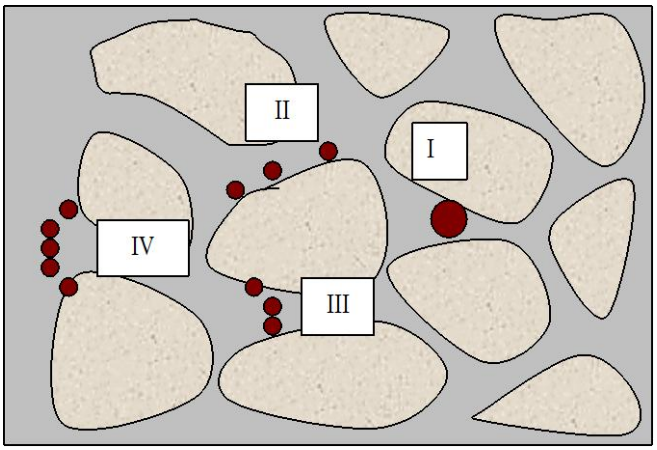

Figure 2.1: Mechanisms of particle retention (Pang, 2007). I. Size exclusion, II. Surface deposition, III. Bridging, IV. Log jam.

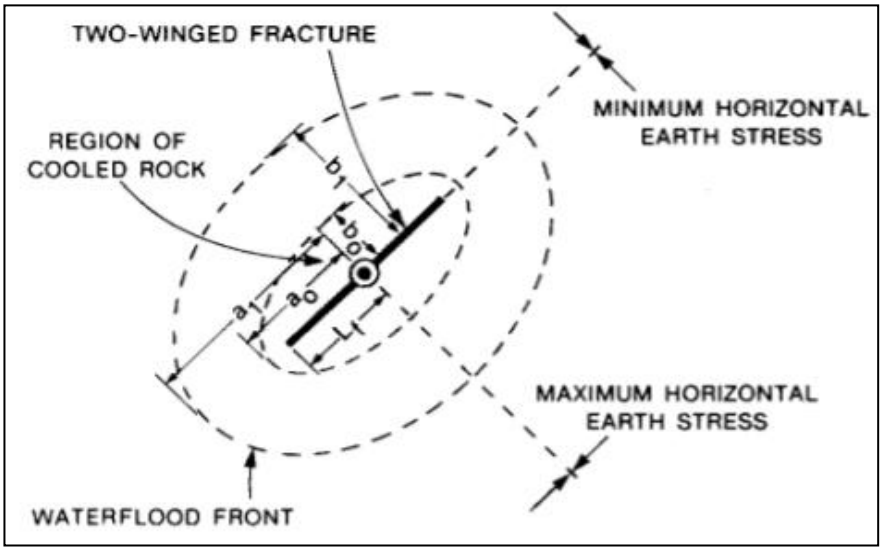

Figure 2.2: Plan view showing a two winged fracture and elliptical thermal and saturation fronts. (Perkins and Gonzales, 1985)

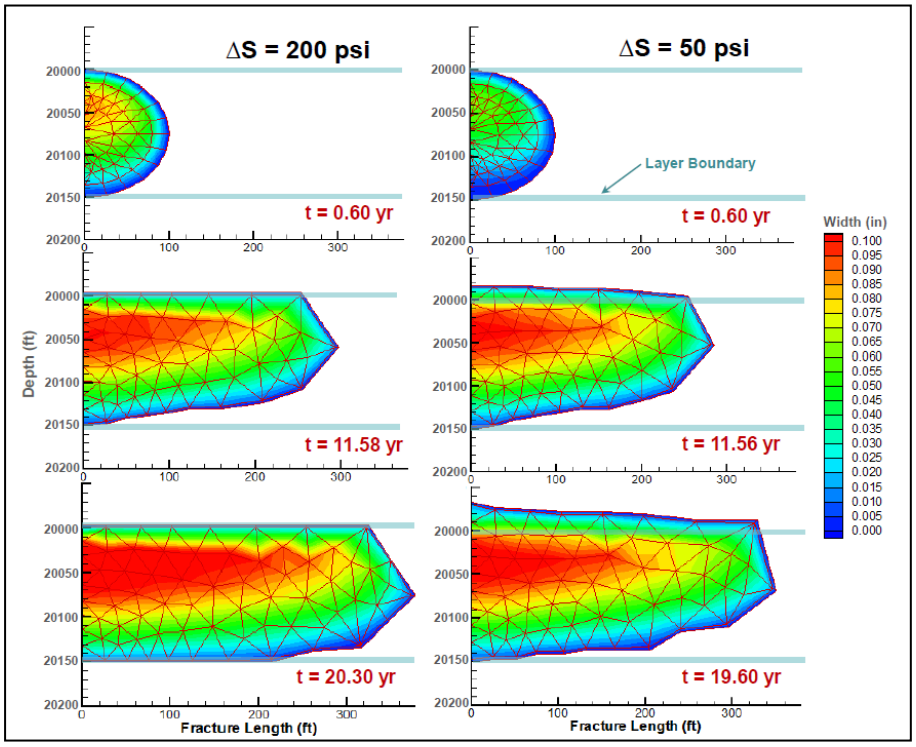

Figure 2.3: Effect of the stress difference between the target and bounding layers on the fracture dimensions. (Hwang, 2014)

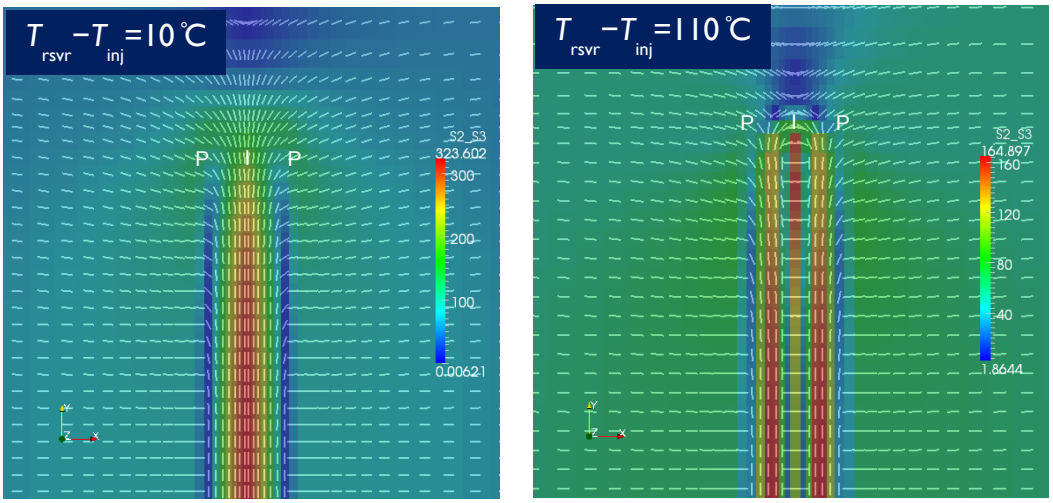

Figure 2.4: Thermoelastic effect of fluid injection in horizontal well pairs. The lines depict the maximum horizontal stress direction. The color depicts the horizontal stress contrast. (Hwang, 2015)

Chapter 3: Model Formulation

Water injection induced fracture propagation and stress reorientation is a combination of several macro (field-scale) and micro level (wellbore-scale) phenomena. Since the near wellbore and far field responses to these processes are coupled, a fully coupled reservoir geomechanics model with dynamic fracture propagation is expected to give a more accurate depiction of the physical process. Hwang et al. (2014) developed a model that showed stress-reorientation during water flooding is dominated by thermal effects as compared to poroelastic effects. However, the model in their work focused on geomechanical effects of depletion and injection but did not account for fracture propagation or particle filtration. This chapter elucidates the development of the model formulation, with an emphasis on the governing equations for pressure, saturation, mechanical displacement and temperature equation. The fracture propagation model and coupled implementation of the particle filtration model is discussed. Subsequently, the coupling of these equations and algorithm implemented to solve the system is discussed (Bhardwaj et al., 2016). The flow model is then verified with a one-dimensional analytical solution.

3.1. METHODOLOGY

The basic framework of the model involves a coupled geomechanics and two phase flow formulation in a three dimensional poro-thermo-elastic reservoir domain. The model was then extended to incorporate propagation of injection-induced fractures. The cohesive zone model was used for arbitrary fracture propagation, where the fracture is fully coupled with the reservoir domain. A dynamic filtration model for permeability reduction was employed on the fracture to incorporate effects of internal damage and

external filter cake build-up due to suspended solids injection. The formulation for arbitrary fracture propagation is based on a finite volume implementation of the cohesive zone model (Bryant et al., 2015), which is coupled with multiphase flow in the reservoir domain. The reservoir domain is allowed to have multiple wells, which can be fractured or unfractured. The model is developed in a modular manner, with flags for effects like fracture propagation, particle filtration, poroelastic and thermoelasticity. This is the first instance where a finite-volume formulation of multiphase flow in the reservoir has been coupled with induced fracture propagation by plugging of suspended solid particles, in a poro-thermo-elastic domain.

The platform chosen for developing the model is OpenFOAM (Field Operation and Manipulation). OpenFOAM is an open source library of continuum mechanics solutions written in C++. Mesh discretization, linear matrix solvers and interpolation schemes available in the library enable discretization of partial differential equations. In addition to numerical and interface features, OpenFOAM also provides a framework to build application-specific boundary conditions and models. Partial differential equations to solve for mass balance, energy balance and stress equilibrium through momentum balance were formulated in the applicable forms for OpenFOAM, and extended to implement numerous models. Pressure (P), water saturation (S_w), mechanical displacement (U) and temperature (T) are the primary unknown field variables that are solved for in each discretized cell of the domain. Boundary conditions and models were created to facilitate implementation of filtration and fracture propagation in multiple wells.

3.2. GOVERNING EQUATIONS

In this work, finite-volume methods (FVM) were employed on a discretized 3-D reservoir domain, to couple the processes of fluid injection, particle filtration, fracture growth and oil displacement. FVM methods have been successfully employed for multi-physics problems and complex system of equations (Jasak and Weller 2000; Tang et al. 2015, Tukovic et al. 2012). The relative ease of implementation makes FVM a good alternative for the numerous coupled aspects involved in water injection. The formulation is based on strong forms of two-phase flow, energy balance, and momentum balance equation and stress equilibrium equations.

3.1.1. Pressure: Fluid flow in porous media

The mass balance equation for immiscible, slightly compressible, two-phase flow in porous media is solved. For a medium with porosity ϕ, Darcy flow is assumed which gives the resulting pressure diffusivity equation as:

$$\phi c_t \frac{dP}{dt} + \frac{\partial}{\partial t}\left(\overline{\nabla} \cdot \mathbf{u}\right) = \overline{\nabla} \cdot \left(\overline{\overline{\lambda_w}} \cdot \overline{\nabla} P\right) + \overline{\nabla} \cdot \left(\overline{\overline{\lambda_o}} \cdot \overline{\nabla} P\right) + B_w \overline{q_w} + B_o \overline{q_o} \tag{3.1}$$

λ_i: Relative Mobility for phase i, i=water, oil.

B_i: Formation Volume Factor for phase i, i=water, oil.

$q_{i:}$ injection/production rate for phase i, i=water, oil.

The pressure equation is coupled with mechanical displacement ($\mathbf{u}$) using Biot's theory of poroelasticity. In Eq. (3.1), c_t is the total compressibility, which takes poroelasticity into account by incorporating the Biot's coefficient (Mainguy and Longuemare, 2002):

$$c_t = (1 - \frac{b}{\phi_o})c_m + S_w c_w + (1 - S_w)c_o \tag{3.2}$$

c_i: Isothermal compressibility, i=water, oil, matrix

b: Biot's coefficient

3.1.2. Water Saturation: Two-phase flow

In order to implement two phase flow, an additional fluid variable, water saturation (S_w) is solved for. The equation for S_w arises from the mass balance for water expressed in terms of saturation and pressure. However, water saturation is coupled explicitly with pressure using the Implicit Pressure Explicit Saturation (IMPES) method. From mass conservation for the water phase:

$$\phi \frac{dS_w}{dt} + \phi S_w \left(c_g + c_w\right) \frac{dP}{dt} = \overrightarrow{\nabla} \cdot \left(\overline{\overline{\lambda_w}} \cdot \overrightarrow{\nabla} P \right) + B_w \overline{q_w} \tag{3.3}$$

Eq. (3.3) is solved explicitly with pressures obtained from Eq. (3.1). For relative permeability modeling, Corey functions have been used for the relation between relative permeability and saturation.

$$k_{rw}(S_w) = k_{rw}{}^{o} \left(\frac{S_w - S_{wr}}{1 - S_{wr} - S_{or}} \right)^{n_w} \tag{3.4}$$

$$k_{ro}(S_w) = k_{ro}{}^{o} \left(\frac{1 - S_w - S_{wr}}{1 - S_{wr} - S_{or}} \right)^{n_o} \tag{3.5}$$

Where,

k_{ri}: Relative permeability for phase i, i=water, oil.

k^o_{ri}: End point relative permeability for phase i, i=water, oil.

S_{ir}: Residual saturation for phase i, i=water, oil.

3.1.3. Temperature: Energy balance

The temperature of the injected water is often relatively lower than the target reservoir. As a result of this temperature difference, there is a sharp temperature front that propagates behind the water saturation front. An energy balance can be written as (Lake, 1989)

$$\begin{aligned}&\rho_b C_{pb}\frac{dT}{dt}+\rho_w C_{pw}\overrightarrow{u_w}\cdot\vec{\nabla}T+\rho_o C_{po}\overrightarrow{u_o}\cdot\vec{\nabla}T\\&=k_b\nabla^2 T+\rho_w C_{pw}\overline{q_w}\left(T-T_{ref}\right)+\rho_o C_{po}\overline{q_o}\left(T-T_{ref}\right)\end{aligned}\tag{3.6}$$

C_{pi}= Specific Heat Capacity i= matrix, oil, water

$\overrightarrow{u_i}$ = Fluid velocity, I = oil, water

k_b= Matrix Conductivity

The temperature is coupled with pressure through the linear fluid velocities in the advection terms of Eq. (3.6).

3.1.4. Mechanical Displacement: Poro-thermo-elasticity

Biot's theory of poroelasticity (Biot, 1955; Detournay and Cheng 1993) has been used to couple the pressure and displacement in the reservoir due to fluid injection and production. A thermal term has been included in the formulation for mechanical displacement based on the formulation by Jaeger et al. (2009). The momentum conservation results in the stress equilibrium (Bryant et al., 2015) which is expressed as:

$$\vec{\nabla}.\left[G\vec{\nabla}\mathbf{u}+G\left(\vec{\nabla}\mathbf{u}\right)^T+\lambda\mathbf{I}tr\left(\vec{\nabla}\mathbf{u}\right)+\sigma_o\right]-\rho\mathbf{f}-b\vec{\nabla}p-(3\lambda+2\mu)\alpha\vec{\nabla}(T-T_o)=0\tag{3.7}$$

G : Shear modulus of rock (Pa)
λ : Lame's first parameter
μ : Lame's second parameter
b : Biot's coefficient

α : Linear thermal expansion coefficient

3.1.5. Cohesive Zone Model: Fracture propagation

The fracture propagation model is based on a cohesive zone implementation for the finite volume domain. This section provides a brief description of the fracture propagation model.

In the current implementation, fractures are treated as physical boundaries to the reservoir domain and are modeled as a physical discontinuity, which can be characterized by a fracture width. Normal and tangential effective traction components are calculated. The components of effective tractions are resolved onto all cell faces and compared to the effective normal σ_{max} and tangential critical stresses, τ_{max}, which are strength related material properties. Only the tensile traction components are included in evaluating the following "failure" criteria:

$$\left(\frac{\| \mathbf{t}_n^{\sigma} \|}{\sigma_{max}}\right)^2 + \left(\frac{\| \mathbf{t}_t^{\sigma} \|}{\tau_{max}}\right)^2 \begin{cases} \geq 1 & \textit{potentially} \text{ a broken face} \\ < 1 & \text{not yet failed} \end{cases} \tag{3.8}$$

Once the face is in the failed region, a cohesive traction is applied on these failed faces. Whether a cohesive traction is applied on a failed face or not is defined by the following criteria based on the Mode I and Mode II surface energy released, or G_I and G_{II} respectively. Only Mode I failure has been considered in the results presented in this work.

$$\left(\frac{G_I}{G_{Ic}}\right) + \left(\frac{G_{II}}{G_{IIc}}\right) \begin{cases} \geq 1 & \text{, face leaves cohesive zone} \\ < 1 & \text{, face remains inside cohesive zone} \end{cases} \tag{3.9}$$

$$t_{cohesive} = \begin{cases} t_{failed}\left(1-\dfrac{\delta}{\delta_C}\right) & \text{, for } \left(\dfrac{G_I}{G_{Ic}}\right)+\left(\dfrac{G_{II}}{G_{IIc}}\right)<1 \\ 0 & \text{, otherwise} \end{cases} \tag{3.10}$$

The implementation for heterogeneous poroelastic formations has been discussed in detail in Bryant et al. (2015), Lee et al. (2015) and Manchanda et al. (2016). Thermal effects have been included in the propagation criteria to account for thermoelasticity.

Stress changes in magnitude and direction, which can be caused by poro-thermo-elastic and mechanical effects of fracture opening and reservoir deformation, are fully accounted for in the model. Multiple fractures in multiple wells, with or without flow distribution can be included along with multiple layers with different mechanical and porous properties to account for heterogeneity (Bhardwaj et al., 2016).

3.1.6. Particle plugging and filtration

Suspended solids in the injected water result in plugging of the near wellbore region and deposition of a filter cake. Particle filtration is a key driving mechanism in the propagation of water injection induced fractures. Injectivity decline and subsequent pressure build-up drives the bottomhole pressure to exceed the fracture gradient in injectors. A dynamic leak-off based permeability reduction model was developed in this work to couple filtration with fracture propagation. The process of filtration is divided into the two stages: initial internal damage, followed by external filter cake build-up.

- Internal Damage Model:

For internal damage, the permeability reduction model proposed by Pang and Sharma, 1997 is used. By solving the mass conservation for a suspension containing particles and assuming rate of deposition to be proportional to the particle concentration

and Darcy velocity, the volume of deposited particles per unit bulk volume, specific deposit ($\sigma_{d)}$ is given as:

$$\sigma_d(x,t) = \lambda_f u t c_{in} e^{-\lambda_f x} \tag{3.11}$$

If ϕ_o is the initial undamaged formation porosity, the corresponding decrease in porosity is expressed by:

$$\phi(x,t) = \phi_o - \sigma_d(x,t) \tag{3.12}$$

The internal damage stops once a critical porosity is reached in the matrix (Wennberg and Sharma, 1997). The time when the transition from internal to external filtration occurs is defined as the transition time and is given by:

$$t^* = \frac{\phi_o - \phi_*}{u c_{in} \lambda_o} \tag{3.13}$$

In the current implementation, it is assumed that internal damage has already occurred once a fracture face is formed. This assumption is made since the transition time is typically very small. Hence all internal damage calculations are made at t=t*.Thus,

$$\begin{aligned} \sigma_d(x) &= (\phi - \phi_o) e^{-\lambda_f x}, t = t^* \\ \phi(x) &= \phi_o - \sigma_d(x) \end{aligned} \tag{3.14}$$

Assuming an undamaged matrix permeability (k_o), the damaged permeability (k_d) can be computed as follows:

$$\frac{k_d}{k_o} = k_{dp} k_{ds} k_{dt} \tag{3.15}$$

- Permeability reduction due to reduced porosity :

$$k_{dp} = \frac{\phi(x)^3 (1-\phi_0)^2}{\phi_0^3 (1-\phi(x))^2} \tag{3.16}$$

- Permeability reduction due to increased surface area :

$$k_{ds} = \left(\frac{1 + \frac{\sigma_d(x)}{1-\phi_o}}{1 + \frac{dg}{dp}\frac{\sigma_d(x)}{1-\phi_o}} \right)^2 \tag{3.17}$$

- Permeability reduction due to increased tortuosity:

$$k_{dt} = \frac{1}{1 + \beta\sigma_d(\mathrm{x})} \tag{3.18}$$

Thus, the internal damage in the formation is a function of the injected particle size, formation grain size and specific deposit. Another important parameter in the internal damage formulation is the filtration coefficient. The internal damage is integrated between the damage radius (x_d) given by Wennberg and Sharma (1997):

$$x_d = (ln2)/\lambda_f \tag{3.19}$$

The internal damaged permeability (k_{int}) is computed between an assumed extended damage radius of $x=3/\lambda_f$ and x=0, where x is the distance from the fracture face to any point in the formation, by numerical integrating the harmonic mean of infinitesimal damage segments :

$$k_{\mathrm{int}} = \frac{(3/\lambda_f)}{\int_0^{3/\lambda_f} \left(\frac{dx}{k(x)} \right)} \tag{3.20}$$

- External Filtration Model:

Filter cake thickness is obtained by a mass balance on the injected particles with the assumption that filter cake build up occurs at the fracture faces only. The leak-off rate across each fracture is computed by using the pressure gradient between the fracture

boundary face and adjacent cells, assuming Darcy flow. Based on the leak-off through each face a filter cake thickness (h_c) is calculated as:

$$h_c = (q_{leak-off} * C_{in} / \rho_p) / (1 - \phi_c) \tag{3.21}$$

A harmonic mean of the matrix permeability, internal damage permeability and external cake permeability is calculated over the adjacent cell center and the fracture face, to get the effective permeability on the fracture face at any given time.

$$k_{eff} = \frac{L}{\frac{h_c}{k_c} + \frac{x_d}{k_d} + \frac{L - x_d - h_c}{k_m}} \tag{3.22}$$

The implementation of a face-wise filter cake build-up is aimed at a more physical representation of the filtration and fracture propagation process. The leak-off at the tip and filter cake build up is a coupled phenomenon. Once a face is broken, filter cake build up commences, leading to permeability reduction by Eq. 3.13. The newly broken faces have maximum permeability and hence the highest leak-off. As a result, filter cake deposition is higher on these faces. As a result, the pressure starts building up inside the fracture due to a reduction in permeability with time, and the fracture propagates again. This continuous process drives fracture propagation in injection wells.

3.3. ALGORITHM

The equations discussed above were discretized in their applicable forms in accordance to the computational fluid and solid mechanics libraries of OpenFOAM, based on C++. Fig. 3.3 illustrates the basic algorithm for the model. There are two distinctive loops in the formulation, the *Time Loop* and the *Failure Loop*. In the current

implementation, pressure and mechanical displacement are iteratively coupled. They are solved implicitly to give pressures in the domain at time t. The fluid flow model is based on an IMPES implementation. The water saturation is solved for explicitly by using pressure dependent relative mobility coefficients computed at $P(t^{n-1})$.The temperature equation is coupled with displacement and pressure through one way coupling. The modularity of the implementation allows for a switch for thermal affects which allows for poroelastic and thermoelastic effects to be studied independently. The residuals are compared against a specified tolerance to check for convergence. Once the system of equations has converged, the magnitude and orientation of the stress field is known for that time step. This is the basic structure of the *Time Loop.* The traction components are then used to evaluate the failure criteria. If the mesh is not updated, i.e. there are no failed faces, the next time step is solved for. In case of failure in the mesh or fracture propagation, the mesh is restructured with physical face detachment for fracture propagation. All field variables are then computed again on the restructured mesh. Permeability is updated on the fracture face based on internal damage and filtration calculation on the failed faces. This is the basic structure of the *Failure Loop*, which is iteratively solved in case of multiple failure events ion the domain, before proceeding to the next time step. The algorithm and formulation are for a three dimensional mesh which can be structured or unstructured.

3.4. NUMERICAL SCHEMES

3.4.1. Upwinding or Upstream weighting

For an IMPES formulation, upstream weighting or upstream differencing or upwinding is known to be conditionally stable. For two-phase flow in a

finite volume discretization, relative mobility of the different phases is calculated at the cell centers, and interpolated at the surfaces or interfaces of the cells. These relative mobility values are numerically upwinded based on pressure gradients in the adjacent cells. The surface interpolated relative mobility of the current cell is based on the direction of fluid flow or pressure gradient. If the pressure of the neighbor adjacent cell is greater than the pressure of the current cell then, the relative mobility interpolated to the surface is from the adjacent neighbor cell and vice versa.

$$\lambda_{rw,surface} = \begin{cases} \lambda_{rw,current} & \text{for } P_{current} \geq P_{neighbour} \\ \lambda_{rw,neighbour} & \text{for } P_{current} < P_{neighbour} \end{cases} \tag{3.23}$$

The hyperbolic nature of the temperature equation makes it necessary to incorporate an upwinding scheme for temperature gradients in convection terms. The stability of the simulation, when thermal effects are included, is strongly dependent on this upwinding scheme.

3.4.2. Adjustable Time Step

The explicit nature of the pressure saturation coupling, requires a smaller time step for stability based on Courant number criteria. However, in later stages of the simulation, when fracture propagation is not very prominent, a time step handling mechanism was used. The time step is updated adaptively based on the maximum water saturation change in the field. When the saturation change is larger than a user specified tolerance value, the time step adaptively becomes smaller to enhance stability.

3.5. VERIFICATION

The poroelastic coupling has been verified with one dimensional Biot's consolidation in Bryant et al. (2014). The verification of the two phase flow model is discussed here. To verify the flow model, the model was verified against the analytical Buckley-Leverett solution for one-dimensional flow. The material balance of a two-phase fluid flow in 1D geometry can be written for a water phase as:

$$\phi \frac{\partial S_w}{\partial t} + u \frac{\partial f_w}{\partial x} = 0 \tag{3.24}$$

where f_w is the fractional flow for water. Assuming no capillarity and no gravity effects,

$$f_w(S_w) = \frac{1}{1 + \frac{k_{ro}\mu_w}{k_{rw}\mu_o}} \tag{3.25}$$

And the velocity of the shock front is obtained as:

$$\left.\frac{\partial x}{\partial t}\right|_{S_w} = \frac{u}{\phi}\left(\frac{df_w}{dS_w}\right) \tag{3.26}$$

The waterflooding shock front can be described by a tangent condition. This condition is that the slope that connects S_{wr} and S_{wf} in f_w vs. S_w curve is the same as the slope at S_{wf}. S_{wf} is the shock front saturation. This determines the value of S_{wf} and can be written as:

$$\frac{\Delta f_w}{\Delta S_w} = \left.\frac{df_w}{dS_w}\right|_{S_w = S_{wf}} \tag{3.27}$$

Using the shock front velocity, the dimensionless distance, x_D can be calculated with the saturation velocity, df_w/dS_w and dimensionless time, t_D. The simulation parameters are listed in Table 3.1.Corey relations are used for relative permeability for oil and water, as shown in Figure 3.4. A rectangular domain of 155m x 15m x 8m is

considered at an initial pressure of 6.9e6 Pa. Wells have been modeled as source and sink terms using the Peaceman well model to correlate rates and pressure. A volume of 9.2e-5 m3/s is injected in the domain for this case. The numerical solution is compared with the analytical solution in Figure 3.5. The numerical solution gives a reasonably good match with the analytical solution, except for the numerical dispersion effects at the shock fronts. An earlier breakthrough in the simulation is also the result of numerical dispersion in the simulation results.

Figures

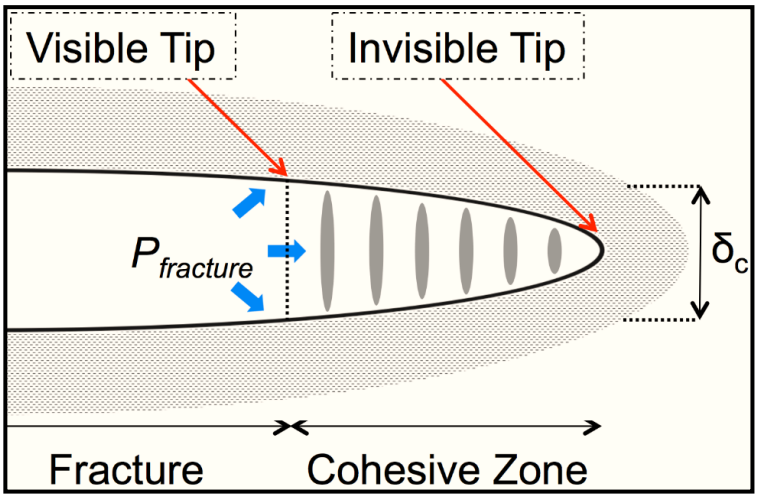

Figure 3.1: Arbitrary fracture propagation in heterogeneous poroelastic formations using FVM based cohesive zone model (Bryant et al., 2014).

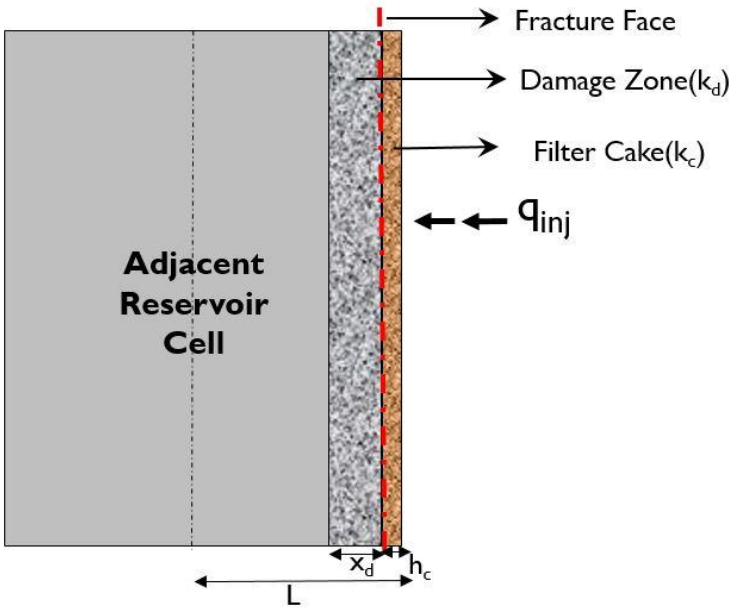

Figure 3.2: Illustration of permeability reduction model implementation in the model.

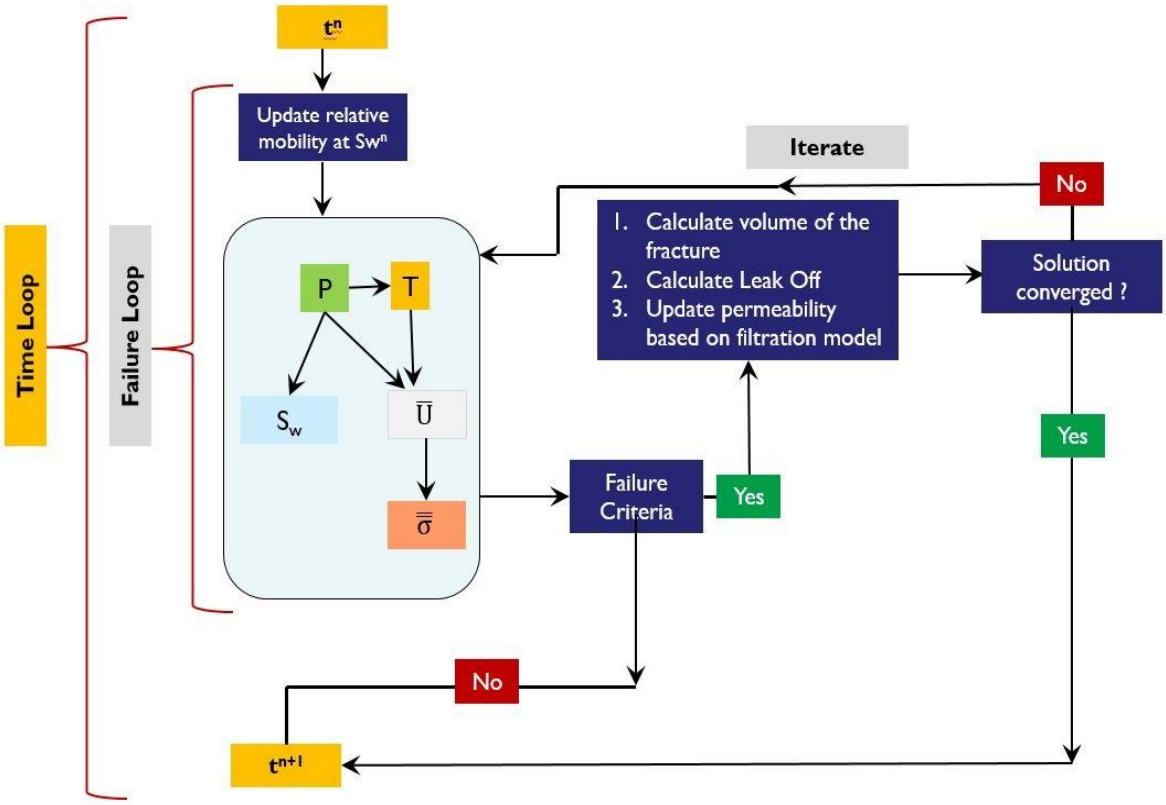

Figure 3.3 Model Algorithm

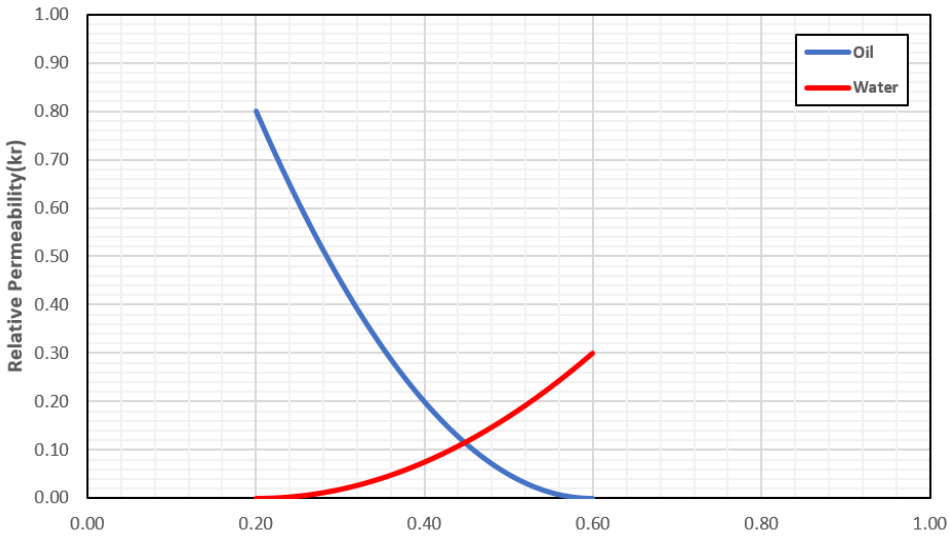

Figure 3.4: Relative permeability curves for oil and water based on Corey functions.

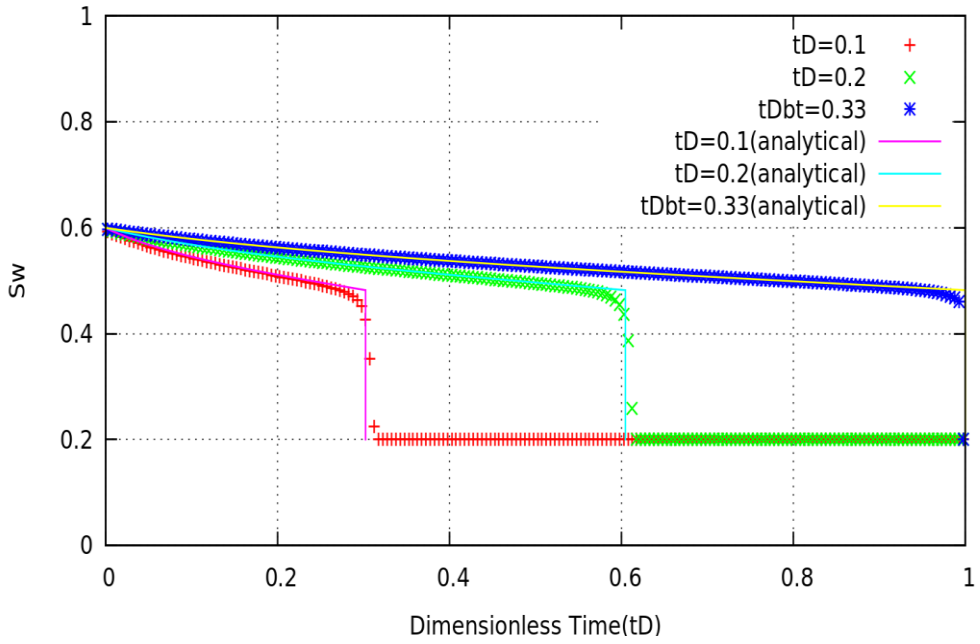

Figure 3.5: Saturation profiles at different dimensionless times for simulated and analytical solutions.

Tables

Table 3.1: Simulation parameters for Buckley-Leverett Validation

Parameter	Value
Residual Oil Saturation	0.4
Residual Water Saturation	0.2
Water End Point Relative Permeability	0.3
Oil End Point Relative Permeability	0.8
Water Viscosity	0.38e-3 Pa-s
Oil Viscosity	1e-3 Pa-s
Water Corey exponent	2
Oil Corey exponent	2

Chapter 4: Results and Discussion

4.1. Effect of particle plugging and filtration

Particle filtration is one of the primary factors affecting induced fracture propagation in water injectors. When the fracture propagates due to plugging , the newly formed fracture faces have the highest permeability and leak-off. As a result of the continuous plugging of the fracture faces, the pressure builds up in the fracture and it propagates further. Hence, fracture propagation and plugging are coupled mechanisms. To examine the effect of particle filtration on fracture propagation, a multi-well case was simulated with different filtration properties in Well 1 and Well 2. All poroelastic effects were considered for this case. The two wells, spaced 100 m apart, are considered in a 250 m x 250 m reservoir domain. The simulation parameters are listed in Table 4.1. The reservoir domain for this case is considered to be two-dimensional. The mesh description, reservoir dimensions and well locations are illustrated in Fig. 4.1.

Fracture Propagation: The results are a combined effect of several phenomena, and are summarized in Fig.4.2. More plugging occurs in Well 2, as a result of the higher concentration of injected particles. As a consequence of the permeability reduction, the pressure build up in Well 2 initiates a fracture first. The pore pressure in the rock matrix increases because of leak-off which increases the compressive stresses on the propagating fracture, due to coupled poroelastic effects. This back-stress can subsequently reduce the width of the fracture. Thus, the fracture in Well 2 is wider due to a smaller volume of fluid leak-off and subsequently smaller back stress.

Ideas expressed in this chapter were first presented in Bhardwaj, P., Hwang, J., Manchanda, R., and Sharma, M. M., 2016. Injection Induced Fracture Propagation and Stress Reorientation in Waterflooded Reservoirs, SPE Annual Technology Conference and Exhibition, 26-28 September, Dubai, UAE, SPE-181883-MS. I was the primary author. Hwang contributed with an initial formulation from his PhD work, which was further developed in collaboration with Manchanda. Sharma supervised the project.

Stress Reorientation: The water saturation profile of the two wells is plotted in Fig.4.3 (a). The water saturation shock front is observed to propagate elliptically in the reservoir, which was at an initial water saturation S_w = 0.2. The maximum horizontal stress direction and pore pressure are shown in Fig. 4.3(b). Thermal effects were excluded for this case. Therefore, stress reorientation is influenced by two factors: the poroelastic effect of fluid injection and the mechanical effect of fracture opening. The poroelastic effect causes stress reorientation in a radially outward direction from the injector, as a result of increased pore pressure and the pore pressure gradient due to fluid injection. Consequently, the reservoir is "pushed" outward. This radial reorientation of the maximum horizontal stress is observed around both the wells, but the reorientation region is larger around Well 2 because of the longer fracture. The mechanical effect of fracture opening is dominant in the region perpendicular to fracture propagation. Due to this effect, a region of complete stress reversal is observed between the two injectors, where the maximum horizontal stress reorients 90 degrees.

4.2. Effect of cold water injection

The thermal effects of cold water injection in a hot reservoir were examined, which is typical for water injection operations in the field. Two scenarios for a single injector well were simulated. The reservoir domain and fluid flow for this case is considered to be three-dimensional. The mesh description, reservoir dimensions and well locations are illustrated in Figure 4.4. Both poroelastic and thermoelastic effects have been considered in this case.

For Case A, the initial reservoir temperature and injected fluid temperature are considered equal at 353K. For Case B, the injected fluid temperature is 293K and the initial reservoir temperature is 353K. Other thermal parameters for the simulation are summarized in Table 4.2. Results for this case are summarized in Figure 4.4. The mechanical displacement vectors and maximum horizontal stress reorientation are plotted for both the cases.

For Case A, displacement vectors and maximum horizontal stress orient radially outwards from the injector due to poroelastic effects. In this case, the reservoir response to fluid injection is completely poroelastic. Additionally, due to mechanical effects, the maximum horizontal stress orients in the direction of fracture opening immediately around the fracture.

For Case B, the displacement and stress response is found to be significantly different since poroelastic effects, mechanical effects and thermoelastic effects are all competing phenomena. In this case, the reservoir response to fluid injection is a combination of poroelastic and thermoelastic effects. In the immediate surroundings of the fracture, displacement is perpendicular to the direction of propagation because the fracture is opening against the minimum horizontal stress. But, as the thermal cooling front propagates from the injector, the displacement vectors begin to orient radially inwards towards the injector. As a net effect, the reservoir is "pulled" inwards towards the injection well.

This observation can be attributed to the effect of thermoelasticity in the cooled region around the injector. When the cold injected water comes in contact with the heated matrix, it causes the matrix to contract. This induces a tensile stress which reduces the magnitude of the compressive stresses in the cooled region. The maximum horizontal

stress orientation in the cooled region is also affected similarly by the induced thermal contraction. Another important effect of the tensile stresses around the fracture in the cooled region is that a longer induced fracture is obtained in Case B. Thus thermal stresses induced by cold water injection can have significant implications on stress reorientation and fracture propagation, and are strongly dependent on the net temperature difference between the reservoir and injected fluid.

4.3. Water breakthrough time in a well pattern

Injection wells are typically placed in patterns with respect to producers, to maximize the efficiency of injection and increase ultimate oil recovery. It should be noted that in a large number of reservoir simulation studies the growth of injection induced fractures is not considered. This is clearly a mistake since most injectors are fractured, whether intentionally or unintentionally. Since, fractures propagate perpendicular to the direction of minimum horizontal stress, well placement relative to initial stress orientation can affect the sweep of the waterflood and breakthrough times. The shape of the waterflood front is governed by the rate of induced fracture propagation, which in turn is driven by particle plugging and permeability reduction due to injected solids and thermal stresses.

A well pattern is simulated to illustrate the combined impact of these phenomena. The reservoir dimensions, well locations are shown in Fig. 4.5 and simulation parameters are summarized in Table 4.3. Production wells P1 and P2 are placed parallel to the direction of maximum horizontal stress, and P3 and P4 are placed in the direction of minimum horizontal stress. Different injection water qualities are considered with injected solids concentration of 0 ppm in Scenario 1 and 20 ppm in Scenario 2.

Stress Reorientation: Pressure profiles and stress re-orientation due to fluid injection and production are shown in Fig. 4.6. Poroelastic effects caused by fluid production, result in the maximum stress being oriented ortho-radially around the production wells. The extent of stress reorientation depends on the initial stress contrast between the horizontal stresses. The maximum compressive horizontal stress decreases around the producer, and reorients perpendicular to the direction of flow. Thus, the maximum horizontal stress reorients around P1 and P2. For P3 and P4, this effect is small as the initial direction of maximum horizontal stress is already perpendicular to the direction of flow. Around the injection well, the maximum horizontal stress is reoriented due competing poro-thermo-elastic effects of fluid injection and mechanical effects of fracture propagation. The poroelastic effect causes the maximum stress to reorient in the radially outward direction. As a result of increased pore pressure due to fluid injection, the reservoir rock can be thought of as being "pushed" outward. The mechanical effect of fracture opening is dominant in the region perpendicular to propagation. Due to this effect, a region of complete stress reversal is observed around injectors, where the maximum horizontal stress reorients 90 degrees to the initial direction. The reorientation region in Scenario 2 is larger due to the longer fracture.

Saturation and Thermal Fronts: The water saturation front and thermal front profiles are shown in Fig. 4.7. In Scenario 1 a short fracture is induced because of a zero injected particle concentration. This occurs due to the initial fluid injection pressure exceeding the tensile strength of the rock. Since the wells are symmetrically placed in the pattern, fracture propagation leads to almost identical water breakthrough in all the production wells. There is slightly earlier breakthrough in P1 and P2, since they are

parallel to the induced fracture propagation direction. The water flood front is observed to be radially uniform. The thermal cooling front has a similar shape but lags behind the waterflood front. The difference in breakthrough times becomes significant in Scenario 2, where a longer fracture is observed due to filtration effects caused by a higher injected particle concentration. Permeability reduction due to plugging and filtration, increases the bottomhole pressure continuously. As a result, a longer fracture is induced over time in Scenario 2. The earlier breakthrough time in P1 and P2 is a consequence of well placement parallel to the direction perpendicular to minimum horizontal stress. The high conductivity channel created by the induced fracture results in an elliptical flood front which is confocal with the fracture. Hence, the aspect ratio of the waterflood will strongly depend on the rate of fracture propagation, which is governed by filtration and plugging effects. The orientation of the front will depend on the placement of wells with respect to the initial maximum horizontal stress direction.

4.4. Stress reorientation and fracture propagation with multiple wells

Stress reorientation occurs in distinct patterns around injection and production wells. However, field development often involves asymmetric well placement. Poroelastic effects will be a result of interaction between the wells as pressure diffuses throughout the field due to depletion and injection. Thermal effects will be limited to regions surrounding the injector since the thermal front is a shock front. Hence, the combined effect of several wells present in the field is expected to govern the stress reorientation. The simulation parameters are listed in Table 4.4.

A simulation of multiple injection wells and producers, with multiple propagating fractures, was performed to illustrate these effects. A 1640 ft. x 1640 ft. x 30 ft. reservoir

is considered with 3 production wells (P1, P2, and P3) and 3 injection wells (I1, I2 and I3). In Fig. 4.8, the pore pressure and the stress orientation are plotted. The stress reorientation regions around injector wells are observed to be bound by the thermal front. An interesting observation is that regions of stress reorientation and even reversal are seen throughout the reservoir and are not limited to near wellbore regions. The spacing of the wells impacts the cumulative effect of stress reorientation, which results from competing effects of production and injection.

Fig. 4.9 shows the thermal front and the displacement vectors in the reservoir. The vectors show focal points of expansion and contraction in the reservoir. In the immediate fracture surroundings, displacement is perpendicular to the direction of fracture due to mechanical opening effects. However, as the thermal cooling front propagates away from the injector, the displacement vectors are observed to orient radially inwards due to contraction induced by cooling. Correctly predicting premature water breakthrough is important for improving the overall efficiency of the water flood. Fig. 4.10(a) and Fig. 10(b) show the final waterflood profile at 50 days and 365 days of injection respectively. The saturation profiles show the unswept region between the producers at the time when breakthrough has occurred in all the three producers after 57 days of injection. Hence, multi-well simulations with dynamic fractures can also be used to identify potentially unswept regions, along with stress reorientation regions, to place infill drilling wells.

4.5. Effect of heterogeneity on flow distribution

For multilayered reservoirs, heterogeneity is a significant factor that governs flow distribution between injection intervals in a vertical well. For example, intra-layer heterogeneity in a sand with different mechanical properties can result in different in-situ

stresses. The effect of initial minimum horizontal stress difference on flow distribution was modeled. A schematic simulation was performed with two layers in a sand with identical properties in Scenario 1 and higher minimum horizontal stress in Layer 2 in Scenario 2. The pressure in the reservoir is assumed to be identical for both scenarios and each layer has identical perforated intervals, from which fluid is distributed from the same wellbore. The mesh description and initial reservoir properties are shown in Fig. 4.11. The simulation parameters are listed in Table 4.5.The resulting flow distribution is shown in Fig.4.12.

In Scenario 1, a homogenous sand is considered with minimum horizontal stress of 13,560 psi in both layers. Consequently, identical induced fracture growth is observed in both the layers. Radial fractures initiate in both layers, which eventually propagate to merge and form a single fracture. The saturation front is illustrated as contours. As a result of symmetric and identical fracture propagation, the water saturation front is also alike in both of the layers. Thus, flow distribution is uniform in the layers and a uniform vertical sweep can be expected in the sand.

For Scenario 2, a heterogeneous sand was considered with a minimum horizontal stress of 14,210 psi in Layer 2 and 13,560 psi in Layer 1. As a result, the fracture propagates primarily in Layer 1. The effective stress is lower in Layer 1, thus making it more conducive to fracture growth in comparison with Layer 2. Once the fracture starts propagating in Layer 1, the flow distribution is preferentially high in Layer 1 as compared to Layer 2. The waterflood front is non-uniform vertically and will result in inefficient sweep in Layer 2, since a preferential flow channel is established in Layer 1. More than 90% of the injected fluid sweeps through Layer 1. Poorer sweep is observed in Layer 2 and this will result in most of the oil in Layer 2 being bypassed leading to

reduction in the overall oil recovery from the reservoir. Thus, heterogeneity can have a significant impact on the flow distribution from a vertical injection well and impact the vertical sweep of the waterflood.

4.6. Effect of stress contrast on fracture containment

Water injection over a long period of time can result in significant in-situ stress reorientation and changes in the stress magnitude caused by thermal and poroelastic effects. The higher pore pressure due to fluid injection, results in a reduction in the stress contrast between the sands and the bounding shale. Thermal effects increase the stress contrast and this results in more contained fractures. Fracture growth into bounding layers will significantly distort all aspects of the mechanical and fluid flow behavior during injection. A simulation was performed with three layers in a shale-sand-shale sequence with a minimum horizontal stress contrast of 50 psi in Scenario 1 and 900 psi in Scenario 2. The results of are shown in Fig. 4.13. Layer properties and reservoir properties are listed in Table 4.6.

The fracture propagates through the bounding shales in Scenario 1, because the stress contrast is relatively low. A higher stress contrast in Scenario 2 results in fracture containment in the target sand. Once a fracture starts to grow into bounding layers, the sweep efficiency of water flooding will be seriously compromised. Thus, it is necessary to predict the potential breach of the fracture into the bounding shale during the planning stage of the waterflood. The fully 3-D fracture propagation model can properly address fracture containment issues and predict growth into bounding layers during injection.

4.7. Waterflooding in a multi-layered reservoir

The cases discussed above clearly show that injection-induced fracture propagation depends on several coupled phenomena. In the field, all these competing effects come into play and have a cumulative impact on the performance of the waterflood. A vertical injection well in a multilayered reservoir was simulated to study the impact of induced fractures on the waterflood profile and oil recovery. The simulation mesh description is given in Fig. 4.14. The simulation parameters are listed in Table 4.7 and layer properties are specified in Table 4.8. The reservoir has 5 layers with an alternating shale-sand sequence where each of the 2 sands is perforated over equal intervals. Two scenarios are considered with 0 ppm injected solids concentration and no thermal effects in Scenario 1 and 10 ppm particle concentration with cold water injection in Scenario 2. The results, a combined effect of several phenomena, are summarized in Fig. 4.15, Fig. 4.16 and Fig. 4.17, with injection time represented in terms of pore-volumes (PV).

Fig. 4.15 shows the fracture with saturation profile in cross-section view for the reservoir and the resulting flow distribution in the two scenarios. The bottomhole pressures are plotted in Fig. 4.16(b). For Scenario 2, due to particle plugging and permeability reduction, the bottomhole pressure increases rapidly and a fracture initiates in Sand 1. As a result of the induced fracture in Sand 1, a preferential flow channel is established, which results in a very non-uniform flow distribution. Thus for Scenario 2, the flow distribution is dominant for Sand 1. For Scenario 1, a more uniform flow distribution is observed which is governed by the product of permeability and thickness of the layers.

The oil recovery and water cut are severely affected when producing from multi-layer reservoirs with non-uniform vertical sweep. Fig. 4.16 (a) shows the cumulative oil production and produced fluid cuts are plotted in Fig. 4.16 (c) and Fig. 4.16 (d). Water breakthrough occurs in Sand 2 followed by Sand 1 for Scenario 1, whereas it occurs much earlier in Sand 1 due to the induced fracture in Scenario 2. The layer-wise fluid production rates are shown in Fig. 4.17. As a result of a premature water breakthrough, oil in Sand 2 is bypassed and a high water cut is obtained. The cumulative oil recovery is 20% higher for Scenario 1, as compared to Scenario 2 after 1 PV of water injection.

Thus, overall waterflood performance is strongly influenced by the induced fracture. This clearly indicates that the sweep efficiency will be adversely impacted when fracture growth occurs in any of the layers. In general, the impact on oil recovery will depend on the rate of fracture propagation, the location of the producers with respect to the induced fracture and layer-wise porous and mechanical properties and stresses. With multiple competing fractures growing in injection wells, simulation of a multi-layered reservoir including the possibility of fractures can help identify and improve conformance control issues.

Figures

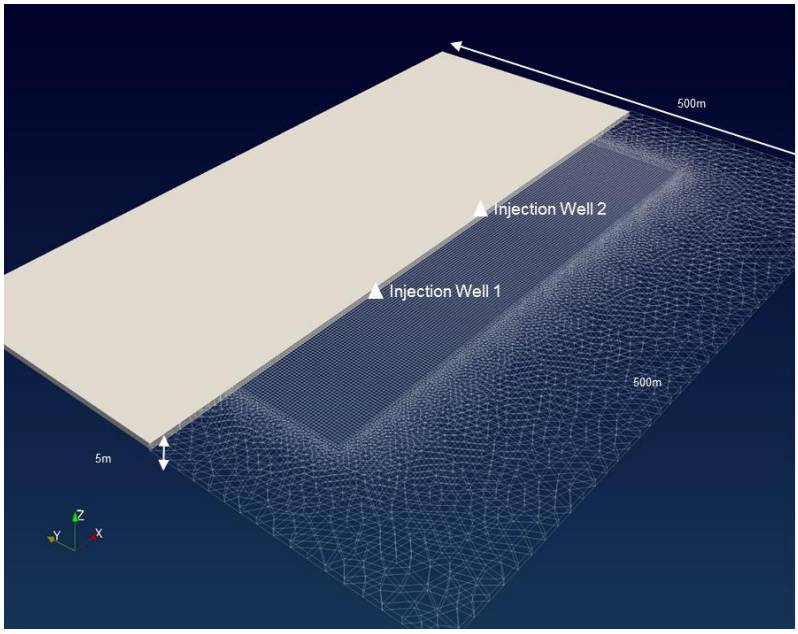

Figure 4.1: Mesh Description for Case 4.1

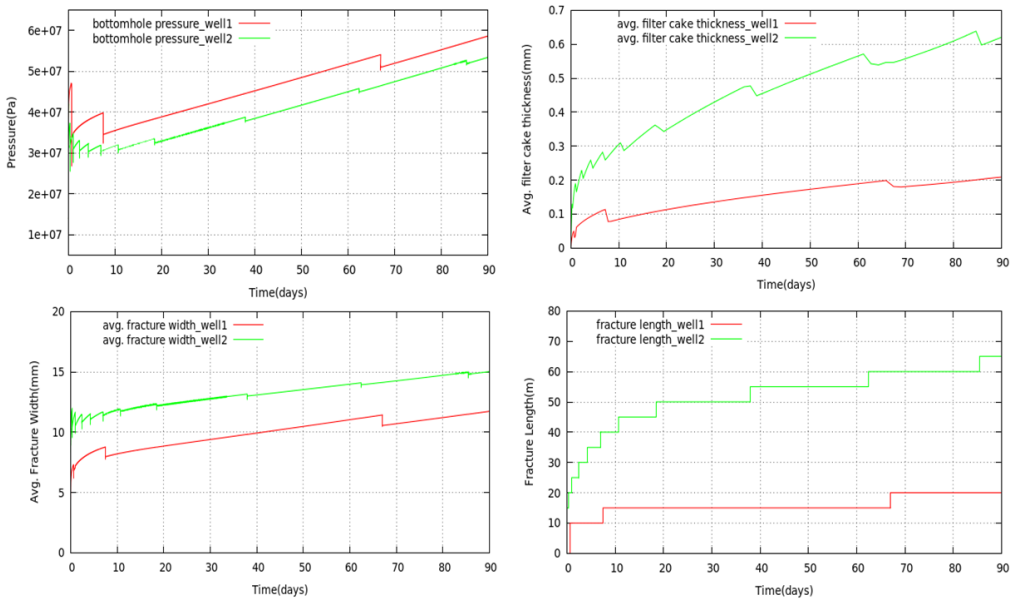

Figure 4.2: (Clockwise from top-left) Bottomhole pressure, average filter cake thickness, induced fracture lengths and average fracture width for Well 1 and Well 2.

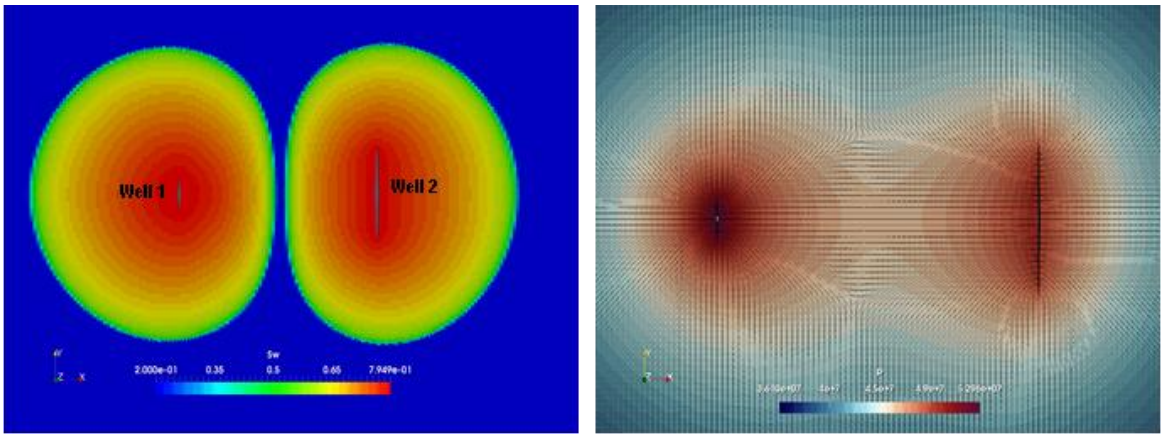

Figure 4.3: (a) Water Saturation front propagation in the reservoir (left). (b)Pore pressure diffusion in the reservoir, with the lines representing maximum horizontal stress orientation (right).

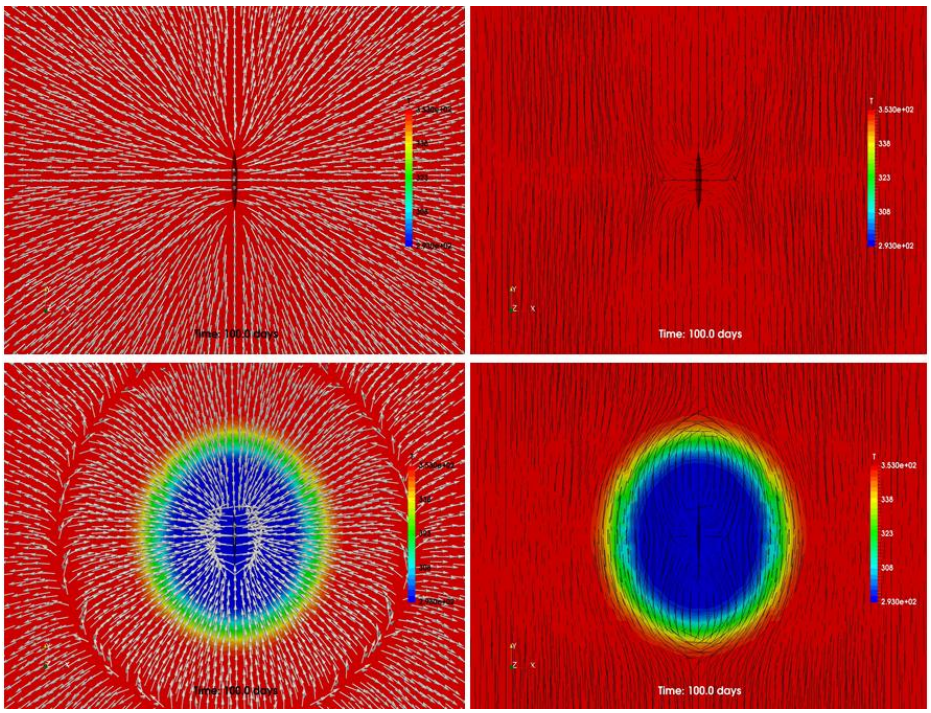

Figure 4.4: Thermoelastic effects on mechanical displacement (arrows) and maximum horizontal stress (black lines) reorientation for Case A (top) Case B (bottom).The colors represents temperature (T).

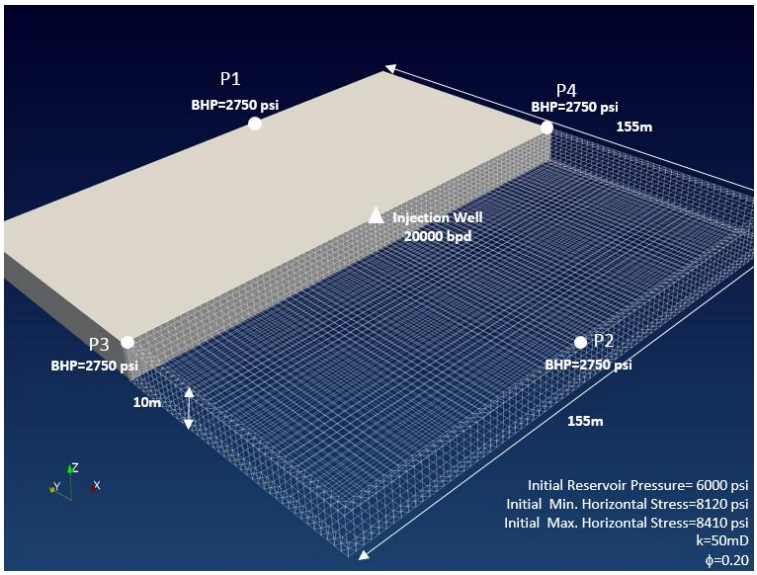

Figure 4.5: Mesh description and initial reservoir parameters for Case 4.2.

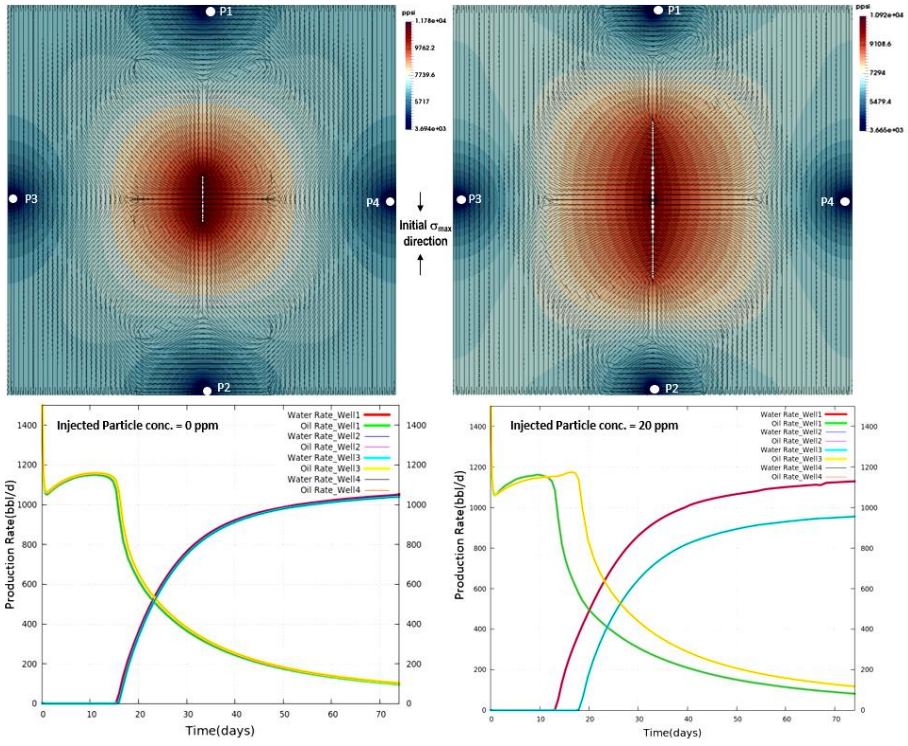

Figure 4.6: Pressure diffusion profile in the reservoir (color). The black lines depict the direction of max. horizontal stress. Scenario 1 (left) and Scenario 2 (right). Fluid production rates (bottom).

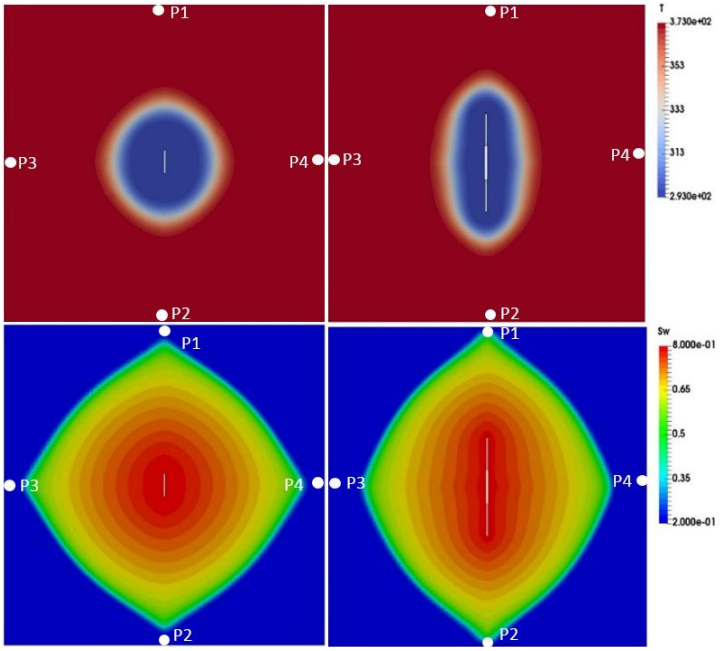

Figure 4.7: Thermal front (top) and water saturation front (bottom) in the reservoir for Scenario 1(left) and Scenario 2(right).

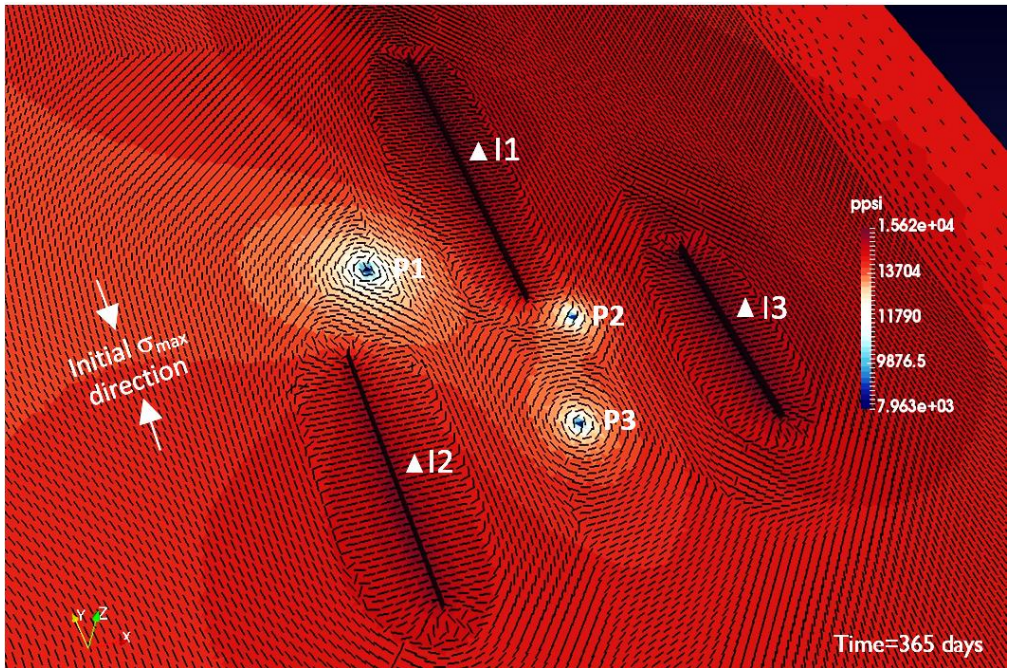

Figure 4.8: Pressure profile in the reservoir (color). The black lines represent the direction of maximum horizontal stress.

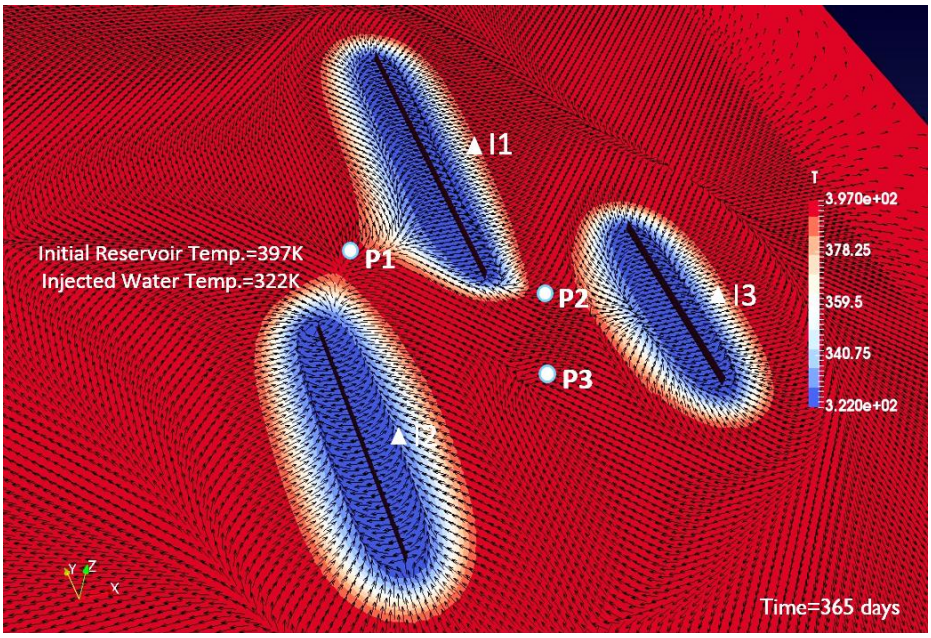

Figure 4.9: Thermal fronts of fluid injection with black arrows representing mechanical displacement vectors.

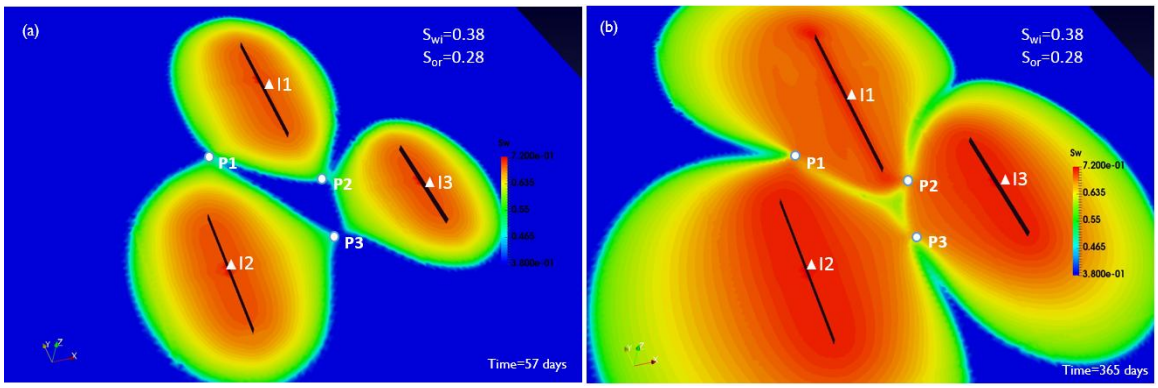

Figure 4.10: (a) Water saturation profiles in the reservoir at t=57 days and (b) t=365 days.

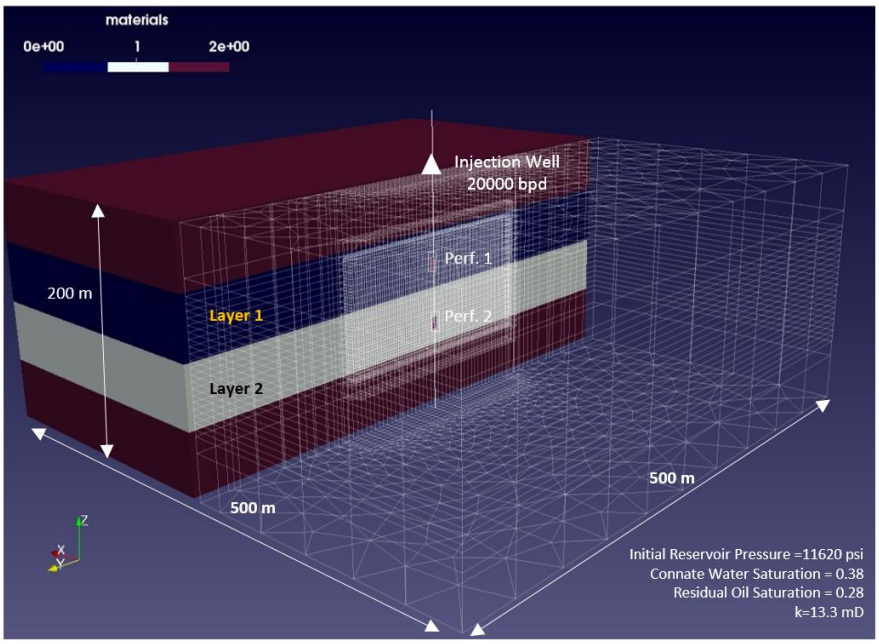

Figure 4.11: Mesh description and initial reservoir parameters for Case 4.5.

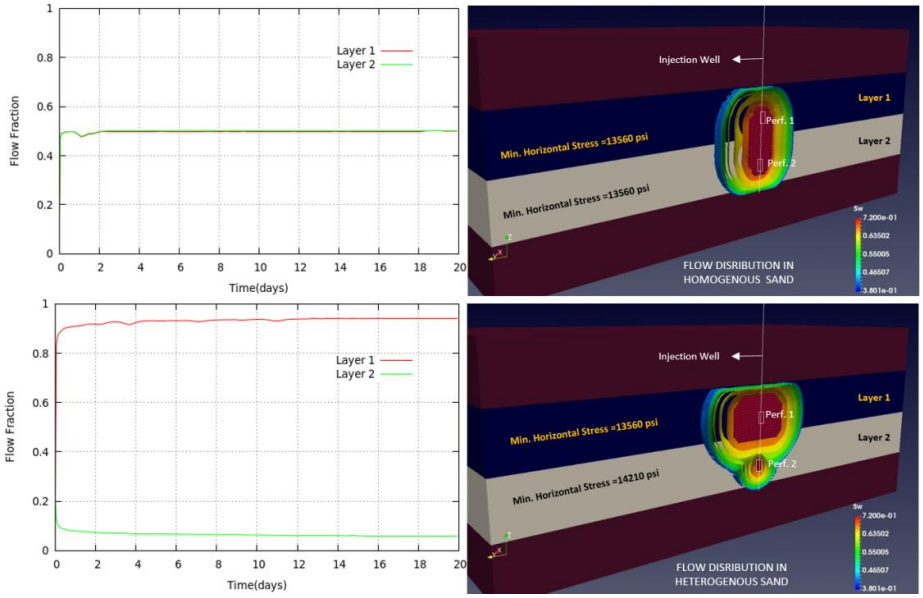

Figure 4.12: Flow distribution plot (left) and water saturation contours (right) for Scenario 1(top) and Scenario 2(bottom)

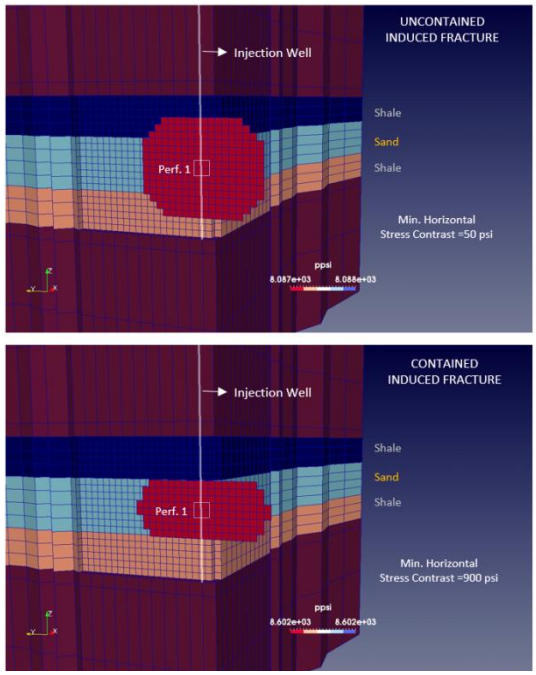

Figure 4.13: Scenario 1(top) and Scenario 2(bottom). Color key shows pressure in the fracture only. Layer colors depict Shale-Sand-Shale sequence.

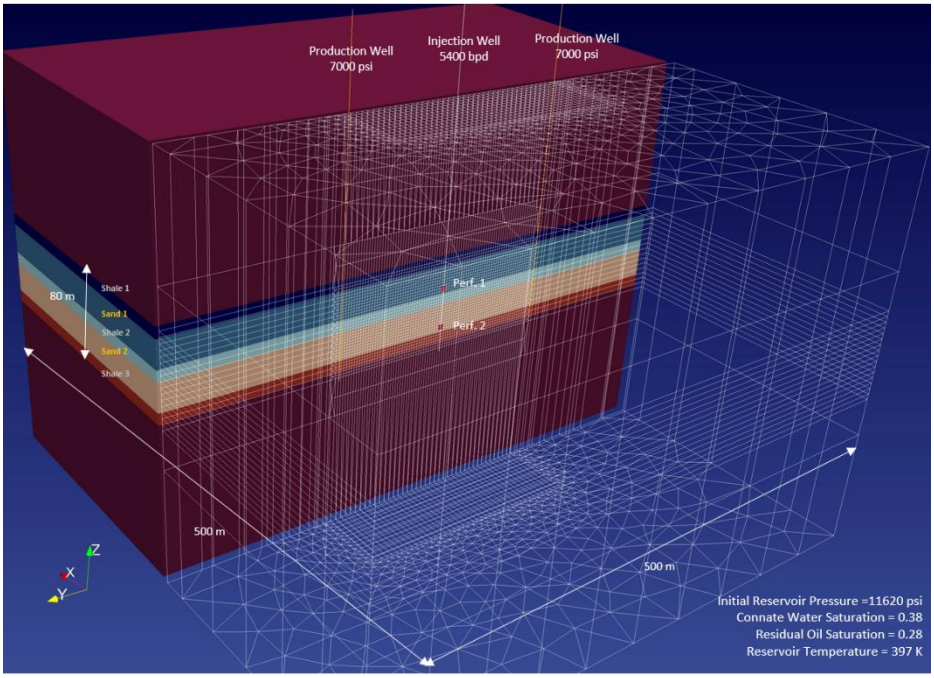

Figure 4.14: Mesh description and initial reservoir parameters for Case 4.7.

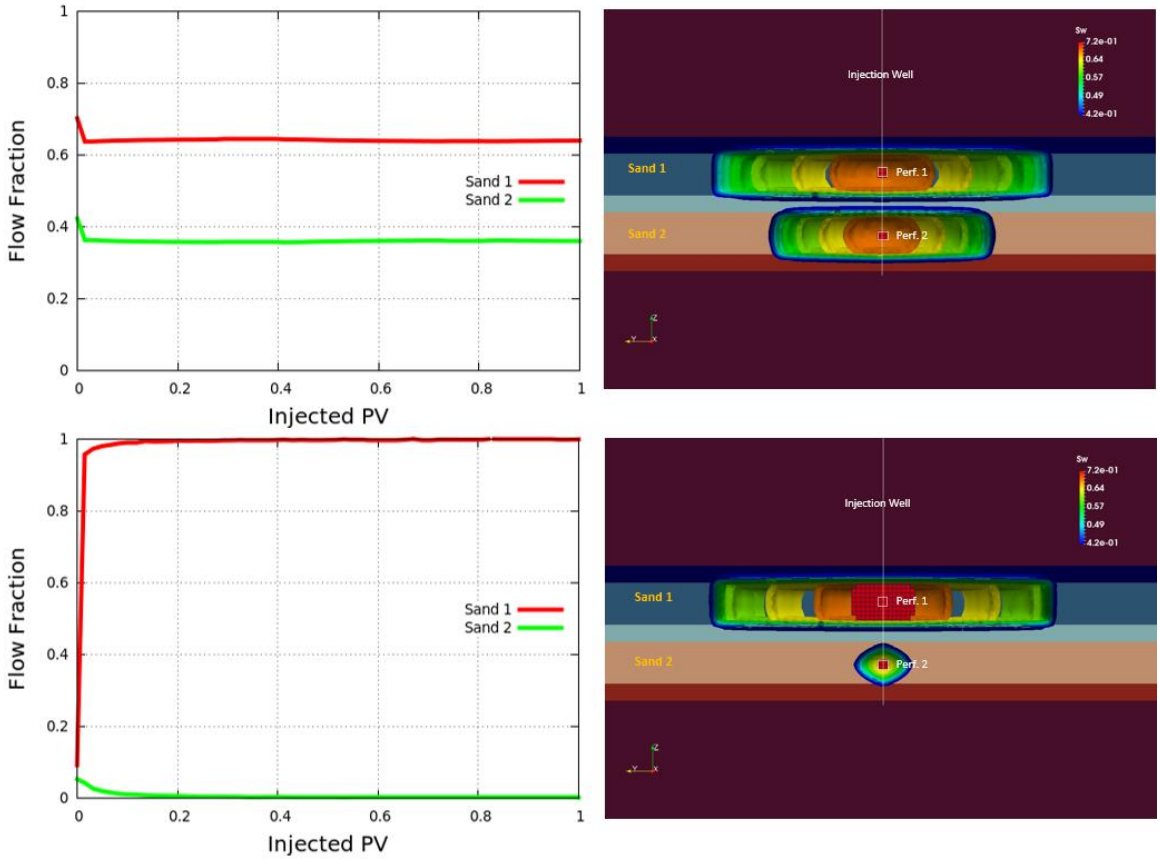

Figure 4.15: Saturation front contours in cross section view (top) and flow fractions in each target layer (bottom) for Scenario 1 (left) and Scenario 2 (right).

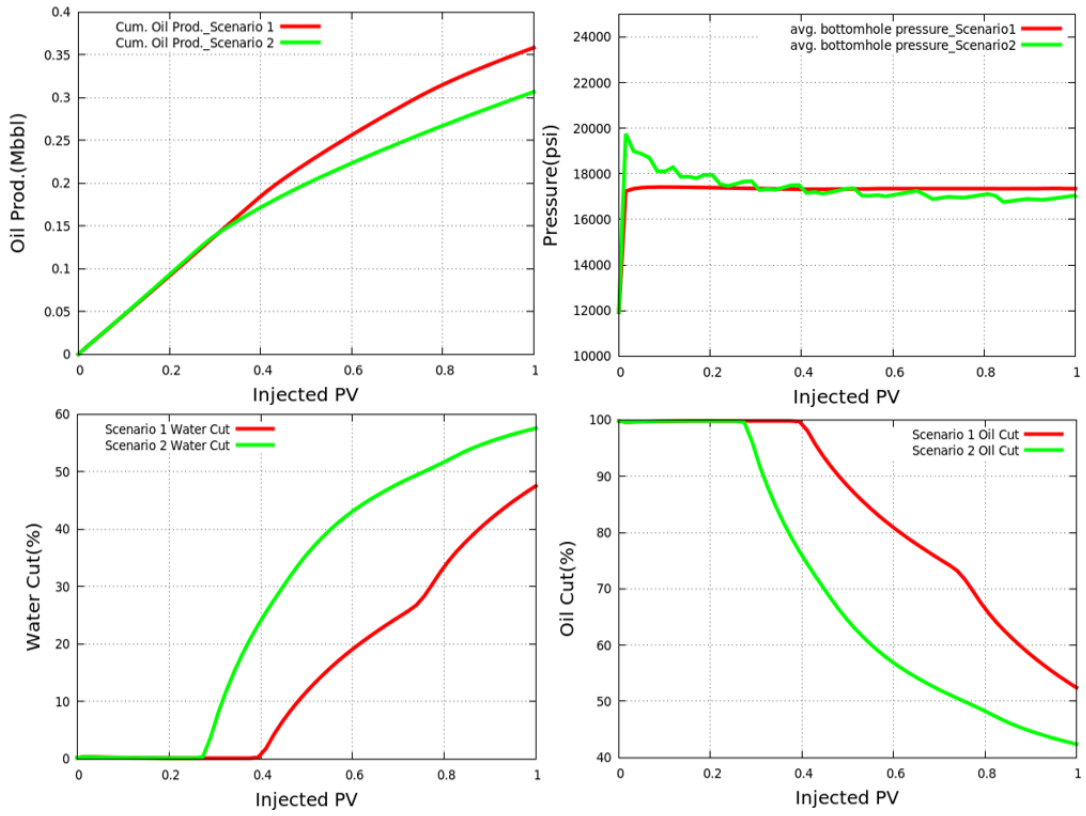

Figure 4.16: (clockwise from top-left) (a) Cumulative oil production (b) bottomhole pressures, (c) oil cut and (d) water cut for Scenario 1 and Scenario 2.

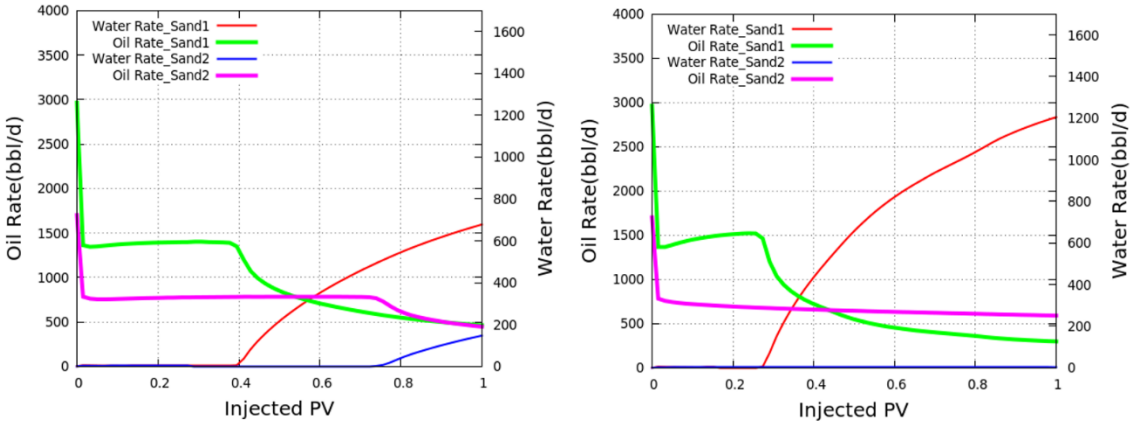

Figure 4.17: Layer-wise fluid production rates (top) for Scenario 1 (left) and Scenario 2 (right). Total rates from all target layers (bottom)

Tables

Table 4.1: Simulation parameters for Section 4.1

Parameter	Value
Reservoir Properties :	
Initial Pore Pressure	1e7 Pa
Maximum Horizontal Stress	2.1e7 Pa
Minimum Horizontal Stress	2e7 Pa
Porosity	0.20
Horizontal Permeability	1e-13 m^2
Biot's Co-efficient	0.6
Young's Modulus	20 GPa
Poisson's Ratio	0.3
Matrix Compressibility	2.6e-9 Pa^{-1}
Fluid Properties :	
Injection Rate	0.01 m^3/s
Water Compressibility	3e-9 Pa^{-1}
Oil Compressibility	3e-9 Pa^{-1}
Water Viscosity	1e-3 Pa-s
Oil Viscosity	5e-3 Pa-s
Filtration Properties :	
Injected Particle Conc. :	
Well 1	10 ppm
Well 2	50 ppm
Filtration Co-efficient :	
Well 1	10 m^{-1}
Well 2	1 m^{-1}

Table 4.2: Thermal simulation parameters for Section 4.2

Parameter	Value
Initial Reservoir Temperature	353 K
Injected Water Temperature	
Case A	353 K
Case B	293 K
Thermal Conductivity :	
Matrix	1.70 W/m-K
Oil	0.15 W/m-K
Water	0.58 W/m-K
Specific Heat Capacity:	
Matrix	0.8 kW/kg-K
Oil	2.4 kW/kg-K
Water	4.1 kW/kg-K

Table 4.3: Simulation parameters for Section 4.3

Parameter	**Value**
Reservoir Properties :	
Initial Pore Pressure	4.137e7 Pa
Overburden Stress	9.5e7 Pa
Minimum Horizontal Stress	5.6e6 Pa
Porosity	0.20
Horizontal Permeability	5e-14 m^2
Biot's Co-efficient	0.6
Young's Modulus	10 GPa
Poisson's Ratio	0.2
Matrix Compressibility	2.6e-9 Pa^{-1}
Fluid Properties :	
Injection Rate	0.04 m^3/s
Water Compressibility	3e-10 Pa^{-1}
Oil Compressibility	3e-9 Pa^{-1}
Water Density	1000 kg/m^3
Oil Density	800 kg/m^3
Water Viscosity	1e-3 Pa-s
Oil Viscosity	5e-3 Pa-s
Relative Mobility Parameters	
Residual Oil Saturation	0.20
Residual Water Saturation	0.20
Water End Point Relative Permeability	0.20
Oil End Point Relative Permeability	0.90
Water Corey exponent	2
Oil Corey exponent	2
Producer Well Properties	
Well Radius	0.1 m
Skin	0
Bottomhole Pressure	1.89e7 Pa
Injected Particle Conc. :	
Scenario 1	0 ppm
Scenario 2	20 ppm

Table 4.4: Simulation parameters for Section 4.4

Parameter	Value
Reservoir Properties :	
Initial Pore Pressure	8e7 Pa
Overburden Stress	1.50e8 Pa
Minimum Horizontal Stress	9.28e7 Pa
Porosity	0.12
Horizontal Permeability	1.5e-14 m^2
Biot's Co-efficient	0.9
Young's Modulus	10 GPa
Poisson's Ratio	0.25
Matrix Compressibility	2.6e-9 Pa^{-1}
Fluid Properties :	
Injected Particle conc.	15 ppm
Water Compressibility	3e-9 Pa^{-1}
Oil Compressibility	3e-9 Pa^{-1}
Water Density	1000 kg/m^3
Oil Density	800 kg/m^3
Water Viscosity	1e-3 Pa-s
Oil Viscosity	5e-3 Pa-s
Relative Mobility Parameters	
Residual Oil Saturation	0.38
Residual Water Saturation	0.28
Water End Point Rel. Perm.	0.225
Oil End Point Rel. Perm.	0.71
Water Corey exponent	2
Oil Corey exponent	2
Injection Rate	
Injector 1	0.012 m^3/s
Injector 2	0.015 m^3/s
Injector 3	0.010 m^3/s
Bottomhole Pressure	
Producer 1	2500 psi
Producer 2	2250 psi
Producer 3	2000 psi

Table 4.5: Simulation parameters for Section 4.5

Parameter	**Value**
Reservoir Properties :	
Initial Pore Pressure	8e7 Pa
Overburden Stress	1.60e8 Pa
Porosity	0.18
Horizontal Permeability	13.3e-15 m^2
Biot's Co-efficient	0.9
Young's Modulus	9.4 GPa
Poisson's Ratio	0.27
Matrix Compressibility	2.6e-9 Pa^{-1}
Fluid Properties :	
Injection Rate	0.04 m^3/s
Injected Particle conc.	10
Water Compressibility	3e-9 Pa^{-1}
Oil Compressibility	3e-9 Pa^{-1}
Water Density	1000 kg/m^3
Oil Density	800 kg/m^3
Water Viscosity	1e-3 Pa-s
Oil Viscosity	5e-3 Pa-s
Minimum Horizontal Stress:	
Scenario 1 :	
Layer 1	9.35e7 Pa
Layer 2	9.35e7 Pa
Scenario 2 :	
Layer 1	9.35e7 Pa
Layer 2	9.80e7 Pa

Table 4.6: Layer properties for Section 4.6

Layer	S_{Hmin}(psi)	k (mD)	E (Mpsi)	Poisson's Ratio
Sand	5220	10	1.15	0.25
Shale	5270 (*Scenario 1*) 6120 (*Scenario 2*)	1e-1	1.45	0.20

Table 4.7: Simulation parameters for Section 4.7

Parameter	**Value**
Reservoir Properties :	
Initial Pore Pressure	8e7 Pa
Overburden Stress	1.6e7 Pa
Matrix Compressibility	2.6e-9 Pa^{-1}
Reservoir Temperature	397 K
Fluid Properties :	
Injection Rate	0.04 m^3/s
Water Compressibility	3e-10 Pa^{-1}
Oil Compressibility	3e-9 Pa^{-1}
Water Density	1000 kg/m^3
Oil Density	800 kg/m^3
Water Viscosity	1e-3 Pa-s
Oil Viscosity	5e-3 Pa-s
Scenario 1:	
Inj. Water temperature	397 K
Injected Particle Conc.	0 ppm
Scenario 2:	
Inj. Water temperature	322 K
Injected Particle Conc.	10 ppm

Table 4.8: Layer properties for section 4.7

Layer Name	*Minimum Horizontal Stress(Pa)*	*Porosity*	*Horizontal Permeability (m^2)*	*Young's Modulus (GPa)*	*Poisson's Ratio*	*Density (kg/m^3)*
Shale 1	1.37e8	0.10	1e-18	25	0.30	2500
Sand 1	9.24e7	0.18	13.3e-15	9.4	0.27	2377
Shale 2	1.40e8	0.10	1e-18	25	0.30	2500
Sand 2	9.35e7	0.19	7.46e-15	9.7	0.25	2368
Shale3	1.39e8	0.10	1e-18	25	0.30	2500

Chapter 5: Conclusion

A new reservoir-scale model, that couples multi-phase flow with geomechanics and dynamic fracture propagation, was developed for multiple wells and multiple induced fractures in injection wells. The filtration of injected solids and oil droplets as well as thermal effects were included to account for the effect of plugging and induced fractures in injectors. In the past such simulations required the use of two separate simulators, one for modeling fracture propagation and the other for conducting the reservoir simulation (including the fracture geometry from the fracturing simulator). The simulator developed in this thesis allows us to do simulate fracture growth, and geomechanical and reservoir flow in one simulator.

Injection induced fractures are a result of various micro and macro-scale physical phenomenon, which are competing effects depending on porous, mechanical and fluid properties of the reservoir under consideration. The model developed in this work also allows for each phenomenon to be studied independently.

- Filtration parameters such as injected particle concertation and filtration coefficient were found to be critical parameters governing the propagation of induced fractures, bottomhole pressures and thus injectivity of the injector wells.
- Thermal contraction of the matrix due to cold water injection was modeled and thermoelastic effects were found to be significant for a large temperature difference between the reservoir and injected fluid. As a result, a longer induced fracture and a lower injection pressure was obtained when thermal effects of cold fluid injection were included.
- The geometry of the waterflood and thermal fronts, were found to be strongly dependent on the rate of fracture propagation, which was shown to be governed by

filtration and plugging effects. The orientation of the front will depend on well placement with respect to the initial maximum horizontal stress direction.

- Stress reorientation due to the competing effects of mechanical displacement, poroelasticity and thermoelasticity were studied around an injector well. For a significant difference in injected water and initial reservoir temperature, thermal effects were found to be dominant in the cooled region.
- For multiple wells, stress reorientation is a field scale phenomenon rather than being limited to near wellbore regions. Since the effect is long range, the combined effect of several wells present in the field is expected to govern the stress reorientation, which results from competing effects of mechanical displacement, poroelasticity and thermoelasticity around producer wells and fractured injector wells. Well placements and injection strategies including injection rate and fluid viscosity selections, require field-scale simulations with multiple and dynamic (time dependent) fracture growth.
- Inter-layer heterogeneity impacts the flow distribution and vertical sweep of the waterflood. The resulting flow distribution was found to be dependent on induced fracture propagation caused by differences in minimum horizontal stress within the sand. A preferential flow channel is created in the layer with lower stress and more favorable material properties for fracture growth.
- Height growth of the induced fracture is governed by the stress contrast between the target sand and bounding layers. As expected, for injection into a single sand bounded by shale layers, fracture containment was seen for higher stress contrast between the target sand and bounding shale whereas the fracture breaches the bounding layers for lower stress contrasts.

- The impact of accounting for induced fracture growth on oil production was examined in a heterogeneous multilayered reservoir. Flow distribution and reservoir sweep were found to be significantly non-uniform for the scenario where a fracture is induced in one of the target sands. A combined effect of layer stresses, heterogeneity in mechanical and porous properties, governs which layer is more conducive to fracturing. The water breakthrough time in each layer and cumulative oil recovery were found to be significantly impacted, with a 20% higher oil recovery for the unfractured scenario, since premature water breakthrough occurs for the fractured case.

The model developed in this work can be used to realistically simulate waterfloods in any field. The ability to monitor the field scale pore pressure and geomechanical response as a result of fluid injection and production during a waterflood allows us to model fracture growth and reorientation on a field-wide scale. This can be used to manage the waterflood, manage injection wells, optimize locations of infill wells and reduce water cuts in producers. In multilayered reservoirs, it is critical to simulate multiple fracture growth and predict a dominant fracture since this will control the vertical flow conformance.

References

Abou-Sayed, A. S., Clifton, R. J., Dougherty, R. L., & Morales, R. H. (1984, January 1). Evaluation of the Influence of In-Situ Reservoir Conditions on the Geometry of Hydraulic Fractures Using a 3-D Simulator: Part 2-Case Studies. SPE Unconventional Gas Recovery Symposium, 13-15 May, Pittsburgh, Pennsylvania. SPE-12878-MS. http://dx.doi.org/10.2118/12878-MS

Bhardwaj, P., Hwang, J., Manchanda, R., and Sharma, M. M. (2016), Injection Induced Fracture Propagation and Stress Reorientation in Waterflooded Reservoirs, SPE Annual Technical Conference and Exhibition 2016, 26-28 September, Dubai, UAE. SPE-181883-MS. http://dx.doi.org/10.2118/181883-MS

Bhardwaj, P., Manchanda, R., Hwang, J., Cardiff, P. and Sharma, M. M. (2016). A New Reservoir Scale Model for Fracture Propagation and Stress Reorientation in Injection Wells, 50th US Rock Mechanics/Geomechanics Symposium. American Rock Mechanics Association, 2016. 23-26 June, Houston, Texas. ARMA-2016-114.

Biot, M.A. 1955. Theory of Elasticity and Consolidation for a Porous Anisotropic Solid. J. App. Phy. 26 (2): 182-185. http://dx.doi.org/10.1063/1.1721956.

Bryant, E. C., Hwang, J., & Sharma, M. M. (2015, February 3). Arbitrary Fracture Propagation in Heterogeneous Poroelastic Formations Using a Finite Volume-Based Cohesive Zone Model. SPE Hydraulic Fracturing Technology Conference, 3-5 February, The Woodlands, Texas, USA. SPE-173374-MS. http://dx.doi.org/10.2118/173374-MS

Detienne, J. L., Ochi, J., & Rivet, P. (2005, January 1). A Simulator Forfor Produced Water Re-injection in Thermally Fractured Wells. SPE European Formation Damage Conference, 25-27 May, Sheveningen, The Netherlands. SPE-95021-MS. http://dx.doi.org/10.2118/95021-MS

Detournay, E., and A.H-D, Cheng. 1993. Fundamentals of Poroelasticity. In Comprehensive Rock Engineering: Principles, Practice and Projects, first edition, ed. J.A. Hudson and C. Fairhurst, Chap. 5, 113-171. Tarrytown, New York: Permagon Press.

Dikken, B. J., & Niko, H. (1987, January 1). Waterflood-Induced Fractures: A Simulation Study Ofof Their Propagation And Effects On Waterflood Sweep Efficiency. Offshore Europe, 8-11 September, Aberdeen, United Kingdom. SPE-16551-MS. http://dx.doi.org/10.2118/16551-MS

Dons, T., Jorgensen, O., & Gommesen, L. (2007, January 1). Seismic Observation and Verification of Line Drive Water Flood Patterns in a Chalk Reservoir, Halfdan Field, Danish North Sea. Offshore Europe, 4-7 September, Aberdeen, Scotland, U.K. SPE-108531-MS. http://dx.doi.org/10.2118/108531-MS

Eylander, J. G. R. (1988, November 1). Suspended Solids Specifications for Water Injection Fromfrom Coreflood Tests. SPE Reservoir Engineering. SPE-16256-PA. http://dx.doi.org/10.2118/16256-PA

Fung, R. L., Vilayakumar, S., & Cormack, D. E. (1987, December 1). Calculation of Vertical Fracture Containment in Layered Formations. SPE Formation Evaluation. SPE-14707-PA. http://dx.doi.org/10.2118/14707-PA

Gadde, P. B., & Sharma, M. M. (2001, January 1). Growing Injection Well Fractures and Their Impact on Waterflood Performance. SPE Annual Technical Conference and Exhibition, 30 September-3 October, New Orleans, Louisiana. SPE-71614-MS. http://dx.doi.org/10.2118/71614-MS

Gu, H. 1987. Study of Propagation of Hydraulically Induced Fractures. Dissertation, The University of Texas at Austin, USA.

Hagoort, J., Weatherill, B. D., & Settari, A. (1980, August 1). Modeling the Propagation of Waterflood-Induced Hydraulic Fractures. Society of Petroleum Engineers Journal. SPE-7412-PA. http://dx.doi.org/10.2118/7412-PA

Hwang, J., & Sharma, M. M. (2013). A 3-Dimensional Fracture Propagation Model for Long-Term Water Injection. American Rock Mechanics Association. 47th U.S. Rock Mechanics/Geomechanics Symposium, 23-26 June, San Francisco, California. ARMA-2013-575.

Jaeger, John Conrad, Neville GW Cook, and Robert Zimmerman. Fundamentals of Rock Mechanics. John Wiley & Sons, 2009.

Jasak, H., and Weller, 2000. Application of the finite volume method and unstructured meshes to linear elasticity. Int. J. Num. Meth. Engg. 48(2):267-287. http://dx.doi.org/10.1002/(SICI)1097-0207(20000520)48:2<267::AID-NME884>3.0.CO;2-Q.

Lake, L.W., 1989. Enhanced Oil Recovery. Prentice Hall Incorporated.

Lee, D., Cardiff, P., Bryant, E.C., et al. 2015. A New Model for Hydraulic Fracture Growth in Unconsolidated Sands with Plasticity and Leak-Off. Presented at

the SPE Annual Technical Conference and Exhibition, Houston, Texas. 28-30 September. SPE-174818-MS. http://dx.doi.org/10.2118/174818-MS

Mainguy, M. and Longuemare, P., 2002. Coupling fluid flow and rock mechanics: formulations of the partial coupling between reservoir and geomechanical simulators. Oil & Gas Science and Technology, 57(4), pp.355-367

Manchanda, R., Bryant, E. C., Bhardwaj, P., & Sharma, M. M. (2016, February 1). Strategies for Effective Stimulation of Multiple Perforation Clusters in Horizontal Wells. SPE Hydraulic Fracturing Technology Conference, 9-11 February, The Woodlands, Texas, USA. SPE-179126-MS. http://dx.doi.org/10.2118/179126-MS

Martins, J. P., L. R. Murray, P. J. Clifford, W. G. McLelland, et. al. 1995. Produced-Water Reinjection and Fracturing in Prudhoe Bay. SPE Reservoir Engineering, 10 (03): 176–182.

Minner, W. A., Wright, C. A., Stanley, G. R., de Pater, C. J., Gorham, T. L., Eckerfield, L. D., & Hejl, K. A. (2002, January 1). Waterflood and Production-Induced Stress Changes Dramatically Affect Hydraulic Fracture Behavior in Lost Hills Infill Wells. SPE Annual Technical Conference and Exhibition, 29 September-2 October, San Antonio, Texas. SPE-77536-MS. http://dx.doi.org/10.2118/77536-MS

Pang, S. and M.M. Sharma, 1997. A Model for Predicting Injectivity Decline in Water-Injection Wells. SPE Formation Evaluation, 12: 194–201. SPE-28489-PA. http://dx.doi.org/10.2118/28489-PA

Perkins, T. K., & Gonzalez, J. A. (1985, February 1). The Effect of Thermoelastic Stresses on Injection Well Fracturing .Society of Petroleum Engineers Journal. SPE-11332-PA. http://dx.doi.org/10.2118/11332-PA

Roussel, N. P., Florez, H., & Rodriguez, A. A. (2013, September 30). Hydraulic Fracture Propagation from Infill Horizontal Wells. SPE Annual Technical Conference and Exhibition, 30 September-2 October, New Orleans, Louisiana, USA. SPE-166503-MS. http://dx.doi.org/10.2118/166503-MS

Sharma, M. M., Pang, S., Wennberg, K. E., & Morgenthaler, L. N. (2000, February 1). Injectivity Decline in Water-Injection Wells: An Offshore Gulf of Mexico Case Study. Society of Petroleum Engineers. SPE Production & Facilities. SPE-60901-PA. http://dx.doi.org/10.2118/60901-PA

Simonson, E. R., Abou-Sayed, A. S., & Clifton, R. J. (1978, February 1). Containment of Massive Hydraulic Fractures. Society of Petroleum Engineers Journal. SPE-6089-PA. http://dx.doi.org/10.2118/6089-PA

Suri, A. and M. Sharma, 2009. Fracture Growth in Horizontal Injectors. Paper SPE 119379 presented at the SPE Hydraulic Fracturing Technology Conference, 19-21 January 2009, The Woodlands, Texas. http://dx.doi.org/10.2118/119379-MS.

Suri, A. and M. Sharma, 2010. A Model for Water Injection into Frac-Packed Wells. SPE Reservoir Evaluation & Engineering, 13: 449–464.

Suri, A., Sharma, M. M., & Peters, E. (2011, August 1). Estimates of Fracture Lengths in an Injection Well by History Matching Bottomhole Pressures and Injection Profile. SPE Reservoir Evaluation & Engineering. SPE-132524-PA. http://dx.doi.org/10.2118/132524-PA

Tang, T., O. Hededal, and P. Cardiff, 2015. On finite volume method implementation of poro-elasto-plasticity soil model. 39(13):1410-1430. http://dx.doi.org/10.1002/nag.2361

Tukovic, Z., A. Ivankovic, and A Karac, 2012. Finite-volume stress analysis in multi-material linear elastic body. Int. J. Num. Meth. Engg. 93(4):400-419. http://dx.doi.org/10.1002/nme.4390

Van Eekelen, H. A. M. (1982, June 1). Hydraulic Fracture Geometry: Fracture Containment in Layered Formations. Society of Petroleum Engineers Journal . SPE-9261-PA . http://dx.doi.org/10.2118/9261-PA

Van Oort, E., van Velzen, J. F. G., & Leerlooijer, K. (1993, August 1). Impairment by Suspended Solids Invasion: Testing and Prediction. SPE Production & Facilities. SPE-23822-PA. http://dx.doi.org/10.2118/23822-PA

Wennberg, K. E., & Sharma, M. M. (1997, January 1). Determination of the Filtration Coefficient and the Transition Time for Water Injection Wells. SPE European Formation Damage Conference, 2-3 June, The Hague, Netherlands . SPE-38181-MS . http://dx.doi.org/10.2118/38181-MS

Wright, C. A., Conant, R. A., Golich, G. M., Bondor, P. L., Murer, A. S., & Dobie, C. A. (1995, January 1). Hydraulic Fracture Orientation and Production/Injection

Induced Reservoir Stress Changes in Diatomite . SPE Western Regional Meeting, 8-10 March, Bakersfield, California. SPE-29625-MS. http://dx.doi.org/10.2118/29625-MS

Yew, C.H. 1997. Mechanics of Hydraulic Fracturing. Gulf Professional Publishing.